



MONASH
University

Reformulating Tension in the Lund String Model of Hadronisation

Honours Thesis

Nicholas Hunt-Smith

Student ID: 26892030

Supervisor: Associate Professor Peter Skands

November 11, 2019

Abstract

Hadronisation is an essential stage of high-energy particle collisions within QCD, describing how quarks and gluons come to produce particles that can be measured by a detector. Motivated by recent observations of discrepancies between popular models of hadronisation and LHC measurements, this thesis revisits some of the theoretical underpinnings of the Lund string model of hadronisation. The goal is to investigate the consequences of a time-dependent string tension, loosely based on recent theoretical work on expanding strings. We find that this modification results in an increased average transverse momentum for strange hadrons compared to non-strange hadrons, which could be observable already in the relatively clean environment of electron-positron collisions.

Acknowledgements

A massive thank you to my supervisor Associate Professor Peter Skands for his continual support throughout my honours year, his knowledge and guidance has been essential in advancing my understanding of physics and scientific writing. I would also like to congratulate my fellow honours students on making it through this very difficult year, and thank them for support and friendship. Thanks as well to Dr Felix Pollock, for a useful discussion on the entanglement of quantum fields.

Contents

1	Introduction	5
1.1	What is Hadronisation?	5
1.2	Beginnings of Strings	7
1.3	Experimental Difficulties	7
2	Basics of Lund String Model	9
2.1	The Yoyo Mode	9
2.2	Lorentz Invariance	11
3	String Fragmentation	12
3.1	Causality	13
3.2	The Schwinger Mechanism	15
3.3	Hadron Distribution Functions	16
4	Thermal String Tension	18
4.1	Motivation	19
4.2	Description	21
4.3	Effects	23
5	Implementation in PYTHIA	27
5.1	Veto Algorithms	27
5.2	Strangeness Ratio	29
5.3	Transverse Momentum	31
6	Results	34
6.1	Proof of Concept	35
6.2	A Realistic Analysis	45
7	Conclusion	48
	Appendices	50
A	Derivation of H and f Distributions	50
B	Lorentz Invariance of Proper Time	51
C	Gaussian Sampling Problem	51
D	UserHook Code	52

1 Introduction

Quantum Chromodynamics (QCD) is an $SU(3)$ gauge theory which models the strong force. The primary method used to tackle QCD is perturbation theory, which can be used to systematically calculate useful values at fixed orders [1, p.17]. For instance, the process of gluon bremsstrahlung (the emission of gluons by quarks) was first proposed as a result of perturbative QCD calculations. The discovery of three-jet events due to gluon bremsstrahlung at the PETRA e^+e^- collider in the 1970s was a resounding confirmation of the existence of gluons, and of the success of perturbative QCD [2].

However, not all interactions in QCD can be modelled as small perturbations. The applicability of perturbation theory is directly related to the coupling- if the coupling is not small, then perturbation theory cannot be applied. A clear example of this issue can be seen in the coupling of the strong force, as calculated from perturbative QCD [3, p.8]:

$$\alpha_s(Q^2) \propto \frac{1}{\ln(Q^2/\Lambda_{QCD}^2)} \quad (1)$$

Q here corresponds to the renormalisation energy scale, while Λ_{QCD} in the above equation has been determined experimentally to be around 0.2 GeV. Renormalisation in quantum field theory is the process of rewriting formulae in terms of measurable quantities, so as to avoid any infinities that arise from using “bare” unrenormalised quantities [4]. The renormalisation scale Q is one of these renormalised quantities. Q is therefore essentially arbitrary, but is usually chosen to be near the energies and momenta being exchanged in a given event so as to minimise the contribution of divergent terms [5].

The size of the strong coupling can be seen to vary significantly with respect to Q , which relates to the energy present in the collision. This sizeable “running” of the strong coupling is a point of differentiation from other field theories such as quantum electrodynamics, which has a coupling that runs much more slowly as energy increases, and with opposite sign [6]. The strong coupling has a clear divergence in the $\ln(Q^2/\Lambda_{QCD}^2)$ term when $Q \simeq \Lambda_{QCD}$. At energies of Λ_{QCD} or lower, the perturbative QCD coupling blows up, indicating the strong interaction can no longer be modelled within this framework.

1.1 What is Hadronisation?

The focus of this thesis is the process of hadronisation, which describes how partons (quarks and gluons) are converted into hadrons (composite particles made of partons) [1, p51]. When partons produced by a collision reach distances of the order of femtometres, their separation (inverse distance) approaches $\frac{1}{r} \simeq Q \simeq \Lambda_{QCD}$. Hadronisation operates at this scale, and therefore requires non-perturbative techniques in order to accurately describe it. In particle colliders, showers of quarks and gluons can be produced by a collision before combining to form hadrons. These hadrons and their decay products can then be detected in the form of

a jet of particles. Understanding hadronisation is therefore essential in order to study the results of particle collisions.

Hadronisation is a direct result of the behaviour of the strong force. From lattice QCD calculations, it is known that there exists a potential between quarks of around 0.9 GeV/fm, or 0.18 GeV² [8, p39]. Lattice QCD is a framework that allows for non-perturbative calculations of the strong force. It does this by dividing space-time into discrete regions and then using discretised quantum fields to computationally measure strong interactions in a static fashion [9]. Evidence for a linearly increasing potential can be seen in the below plot of the QCD potential [10]:

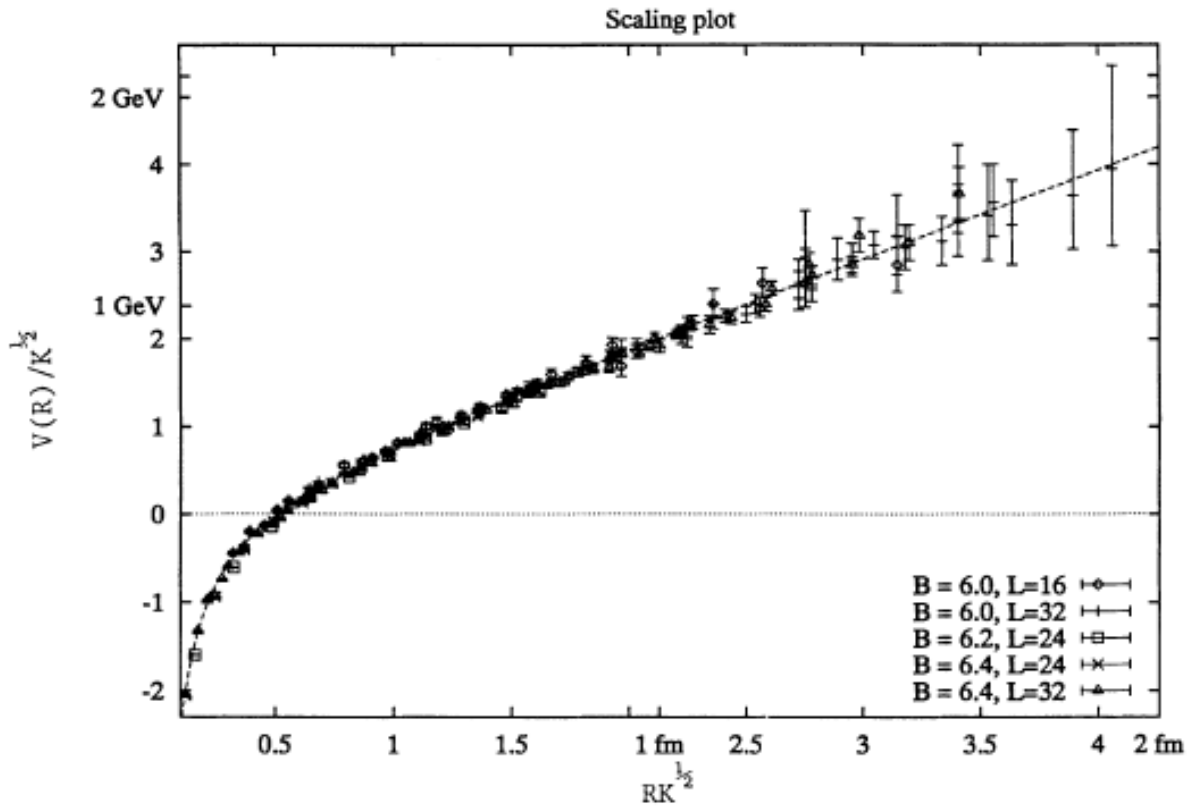


Figure 1: Plot of QCD potential as a function of separation between quarks using lattice QCD. The legend on the bottom right refers to lattice parameters that are beyond the scope of this thesis.

Figure 1 corresponds to the potential between a static quark-antiquark pair placed on a lattice. The axes are scaled by units of the string tension $\sqrt{\kappa} = 420$ MeV. A constant V_0 has been subtracted from every point, and the dashed line is given by $V(R) = R - \frac{\pi}{12R}$. This plot is generated in the quenched approximation, when the string is not allowed to break. Even at relatively short distances, it is clear that the potential between two quarks has an increasingly linear form. As such, as quarks are moved further apart from one another, the potential between the quarks also increases, which is equivalent to a “strong” force pushing the quarks back together.

This essential aspect of QCD is called *quark confinement*, explaining why quarks are held together in hadrons rather than existing individually in a stable state. There currently exists no formal mathematical proof for quark confinement, despite the experimental fact that quarks have never been observed directly in an isolated state [7]. This problem forms part of the Yang-Mills Millennium Prize, for which there is a million US dollar reward for anyone who can find a correct solution.

A necessary aspect of confinement is that any quark-antiquark pairs created experimentally will experience increasingly large potential as they move apart. If the separation and resulting potential is large enough, quark-antiquark pairs can be created [11]. This in turn results in cascades of hadrons as the created quarks combine in a process called hadronisation.

1.2 Beginnings of Strings

One way in which non-perturbative modelling of hadronisation was developed is the Lund string model [12]. Built on ideas from Artru and Mennessier in the 1970's [13], the Lund Model represents the strong force field spanned between two quarks by a string stretched between them. In doing so, the force pulling quarks together is described by the potential of a string:

$$V(r) = -\kappa r, \tag{2}$$

with a string tension κ . This string tension is a constant, so the potential increases linearly as the particles are pulled further apart. The potential therefore replicates the form seen in figure 1 at large separations. In this way, the complex field-theoretic interaction between quarks is simplified to that of a 1+1-dimensional string object.

In order to compare the Lund Model to observation, the mathematical underpinnings of the model were implemented in the form of computer code within Monte Carlo event generators. Monte Carlo event generators are widely used to simulate particle physics events that are too complicated to be calculated directly. This is done by splitting the overall unsolvable event into individually solvable stages, which are then connected probabilistically using Monte Carlo mathematical methods [14]. One of these stages is hadronisation, with popular event generators such as PYTHIA [15] using the theoretical framework of the Lund Model. Comparisons between the predictions of these event generators and experimental results have generally favoured the Lund string model, ever since early gluon jet measurements of electron-positron collisions in 1979 by the JADE detector at the PETRA collider [16].

1.3 Experimental Difficulties

However, recent observations in proton-proton collisions at the Large Hadron Collider (LHC) are not as well described by the Lund model. In particular, measurements show that a higher amount of strange hadrons is being produced than is predicted by event generators such as

PYTHIA. A strange hadron is any hadron that contains a strange quark. The enhanced strangeness has been seen clearly in the ALICE detector at the LHC, from which the below graph was generated [17]:

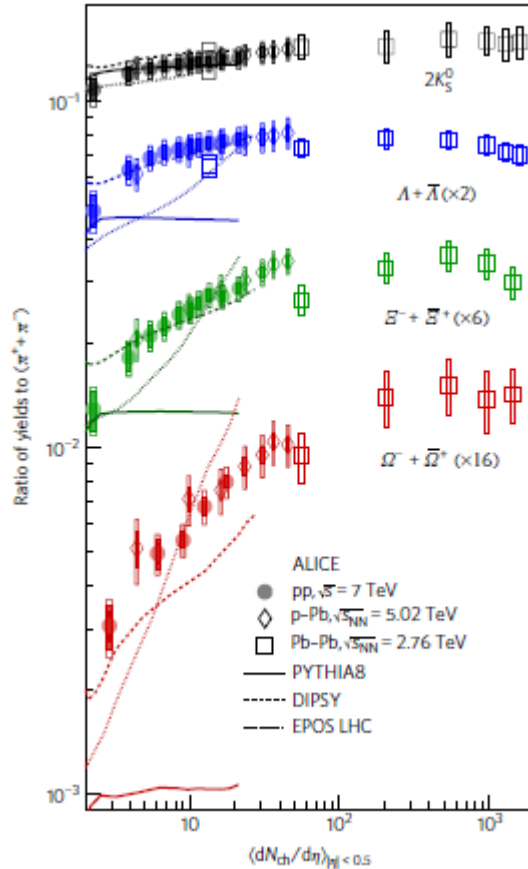


Figure 2: Plot of ratios of strange particle yields to pion yields as a function of particle multiplicity.

Here, the number of strange particles detected is plotted on the y axis as a ratio of the number of pions detected. On the x axis is the particle multiplicity, or the number of charged particles that were produced in the collision. The different coloured data corresponds to different types of strange hadrons. The solid circles represent the experimental data obtained from proton-proton collisions at the LHC, and the solid lines are the predictions made by PYTHIA. For each particle species, the experimental data indicates that there should be increasing yield ratios of strange particles as particle multiplicity increases, as shown by the upward trend in the red, green and blue data points. This is not reflected in PYTHIA, which predicts a flat line in each case. The cause of this difference is the fact that the Lund model does not incorporate any interaction between nearby strings. If there are more particles around, as in high multiplicity events, then there are also more strings around in the hadronisation stage. Since the strings in the Lund model are unaffected by any strings nearby, there is no reason why an increase in particle multiplicity should change any of the Lund model's predictions. Hence, PYTHIA tells us to expect a value for the hadron yield ratio

that is independent of particle multiplicity, and we see a constant line in the above plot.

Given this anomaly in the predictions by PYTHIA, there is clear motivation to revise the Lund string model on which PYTHIA is partly based. Specifically, in this project we will be considering possible differences between the static $q\bar{q}$ lattice QCD potential and that of a dynamically expanding string. This is not intended to explain the ALICE measurements by itself, but is an important step towards a greater understanding of how strange particles are produced in hadronisation.

2 Basics of Lund String Model

2.1 The Yoyo Mode

A full description of the Lund string model is required before any modifications can be considered. The simplest scenario within the Lund model is that of a stable meson, consisting of a quark-antiquark pair. Under the Lund model, the quarks are represented as oscillating back and forth continuously with a string extended between them. The string has a constant tension κ . This is called the *Yoyo mode*, and is depicted below [18]:

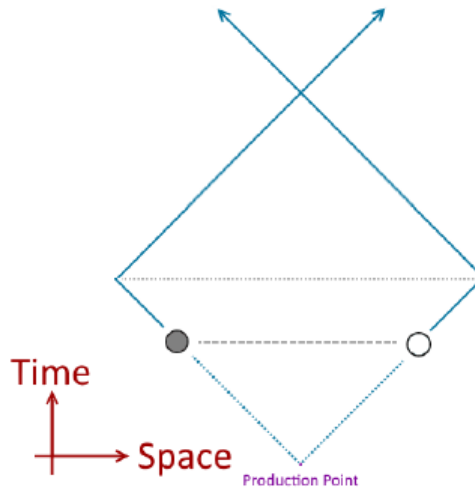


Figure 3: Light cone diagram of a stable meson in Lund String model.

Figure 3 is an idealised light cone diagram in which the quarks are assumed to have no mass, and to therefore propagate at the speed of light. As the quarks move apart, their kinetic energy is converted into potential energy stored in the string, until they become stationary and begin to move back towards one another.

The underlying mathematics of this picture starts from the assumption that the quarks are under the influence of a constant force κ , equal to the string tension. This assumption

is based on the linear potential from eq.(2). For a single relativistic quark of rest mass m , a force equation can be formed [19, p.115]:

$$\frac{dp}{dt} = -\kappa, \quad (3)$$

This differential equation has the solution:

$$p(t) = p_0 - \kappa t = \kappa(t_0 - t). \quad (4)$$

One of Hamilton's equations of motion from classical mechanics is:

$$\frac{dx}{dt} = \frac{dE}{dp} = \frac{p}{E}, \quad (5)$$

E is here the relativistic particle energy, given by:

$$E = \sqrt{p^2 + m^2}. \quad (6)$$

Using the chain rule, the change in energy with respect to the spatial coordinate is:

$$\frac{dE}{dx} = \frac{dE}{dp} \frac{dp}{dt} \frac{dt}{dx}, \quad (7)$$

From eq.(5), $\frac{dE}{dp} \frac{dp}{dx} = 1$, so:

$$\frac{dE}{dx} = \frac{dp}{dt} = -\kappa, \quad (8)$$

This differential equation has the same solution form as for momentum:

$$E(x) = E_0 - \kappa x = \kappa(x_0 - x). \quad (9)$$

The spatial coordinate x is related to the separation of the quarks (r) by $r = 2x$. Neglecting the factor of 2, eq.(9) replicates the form of eq.(2), thereby obtaining a linear potential as is expected. Substituting solutions for energy and momentum into eq.(6), we have:

$$m^2 = E^2 - p^2 = \kappa^2[(x_0 - x)^2 - (t_0 - t)^2]. \quad (10)$$

Eq.(10) defines a hyperbola in space-time, with intersection between asymptotes at (t_0, x_0) . The turning point of this hyperbola is positioned a distance $\frac{m}{\kappa}$ from this intersection. The turning point occurs when momentum is equal to zero, which is at $t_0 = \frac{E_0}{\kappa}$ according to eq.(10). Visually, this looks like:

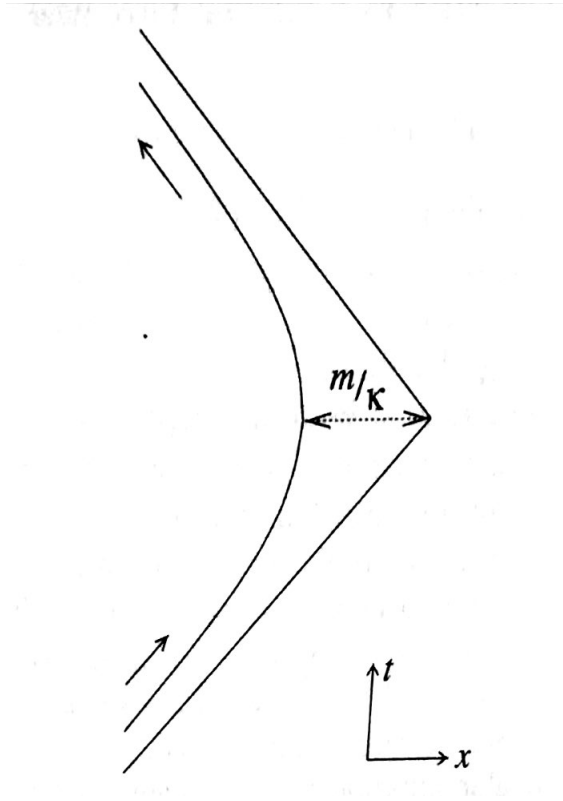


Figure 4: Hyperbolic motion of a massive quark under a constant force κ .

If the mass of the quark is set to zero then eq.(10) implies $(x_0 - x) = (t_0 - t)$. This means the quark moves directly along the asymptotes depicted in figure 4. If we now consider a second massless quark moving in the $-x$ direction, the light cone diagram becomes the same as the Yo-yo mode in figure 3. Light cone diagrams from now on will represent quarks as being massless for visual simplicity, so that they move in straight lines rather than in a hyperbolic fashion.

2.2 Lorentz Invariance

A crucial aspect of this model is that it is Lorentz invariant. Assume that in the original frame $x = \pm t$ and $E = \pm p$. Under a Lorentz boost β in the positive x direction (only longitudinal boosts are considered here), time and momentum transform as [8, p.40]:

$$t' = \gamma(t - \beta x) = \gamma(1 \mp \beta)t, \quad (11)$$

$$p' = \gamma(p - \beta E) = \gamma(1 \mp \beta)p, \quad (12)$$

Therefore:

$$\kappa' = \frac{dp'}{dt'} = \frac{dp}{dt} = \kappa, \quad (13)$$

So the string tension is unchanged under a Lorentz boost. The total area spanned by the string in one period is also invariant under a Lorentz boost. This can be seen by considering the area spanned by the string for the Yo-yo mode in figure 3. By dividing the area into 8 equilateral triangles of side length $t_0 = \frac{E_0}{\kappa}$, the area must be equal to:

$$A = 8 \left(\frac{1}{2} \right) \left(\frac{E_0}{\kappa} \right) \left(\frac{E_0}{\kappa} \right) = 4 \frac{E_0^2}{\kappa^2} = \frac{m^2}{\kappa^2} \quad (14)$$

Since m is the invariant mass and κ has been shown to be invariant under a Lorentz boost, the area must be Lorentz invariant as well. Pictorially, a boost in the negative x direction can be represented as [20]:

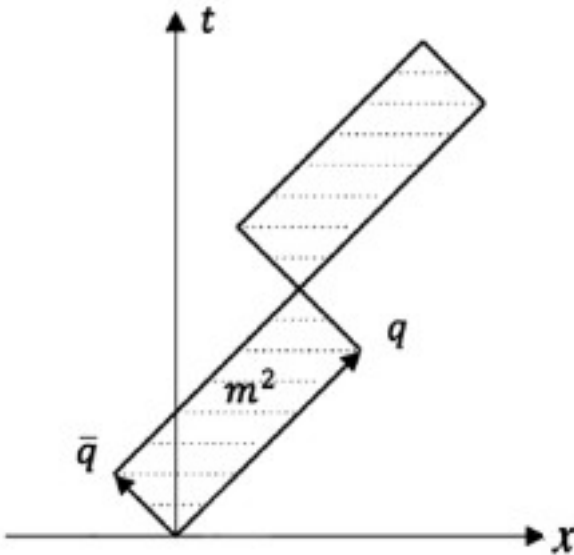


Figure 5: Yo-yo mode in a boosted frame along negative x direction.

A Lorentz boost in a direction corresponds to slanting the usual light cone diagram in the opposite direction, conserving the area spanned by the string.

3 String Fragmentation

Up until this point, the addition of a string within the Lund model might seem unnecessary. Stable hadrons could be perfectly well described by just a force field between quarks that increases as they move apart, without invoking a string tension at all. However, a key aspect of a string is that it can break if it is stretched enough. For the Lund model, these string breaks correspond to the decay of the string state into a pair of smaller strings via the creation of a new quark-antiquark pair. This is intended to reflect experimental observations, which demonstrate that quark-antiquark pairs with higher energy than that of stable hadrons will decay into particles with smaller mass [21]. A visual representation of these string breaks is shown below [19, p.140]:

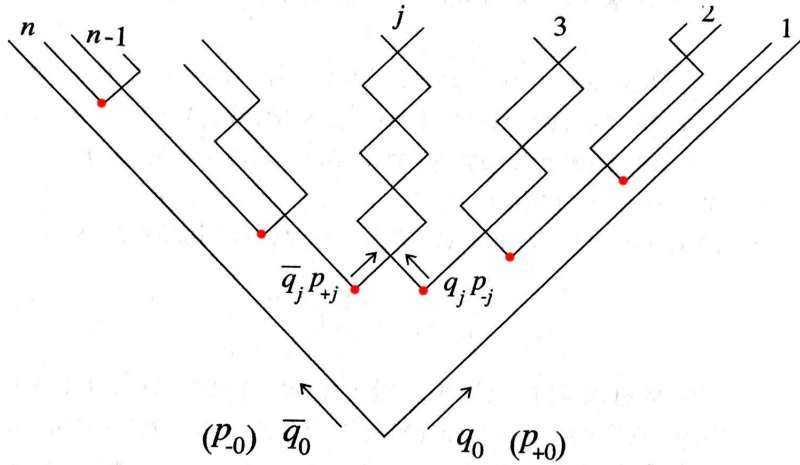


Figure 6: Light cone diagram of multiple string breaks.

The initial quark-antiquark pair are moving with equal momentum in opposite directions, with too much energy to exist as a single stable hadron in the Yoyo mode. The string stretched between them must therefore break. Each red dot on this diagram corresponds to a string break and the creation of a quark-antiquark pair. These points are named *vertices*, and the overall diagram is describing the process of *string fragmentation*. There is no limit to the number of string breaks that can occur as long as there is enough energy available, and the breaks need not be symmetric even if the original quarks have equal and opposite momentum.

In this case, the string initially breaks in two places, with two sets of quark-antiquark pairs created. Further string breaks may occur if the energy contained in the string fragments is high enough, otherwise the quarks will join together in the Yoyo mode. The numbered states in the Yoyo mode depicted in figure 6 therefore correspond to stable hadrons. In essence, figure 6 describes how we can go from a single quark-antiquark pair into a cascade of observable hadrons that can be detected experimentally as a particle jet.

3.1 Causality

Consider now a single string fragment of the previous process, shown below:

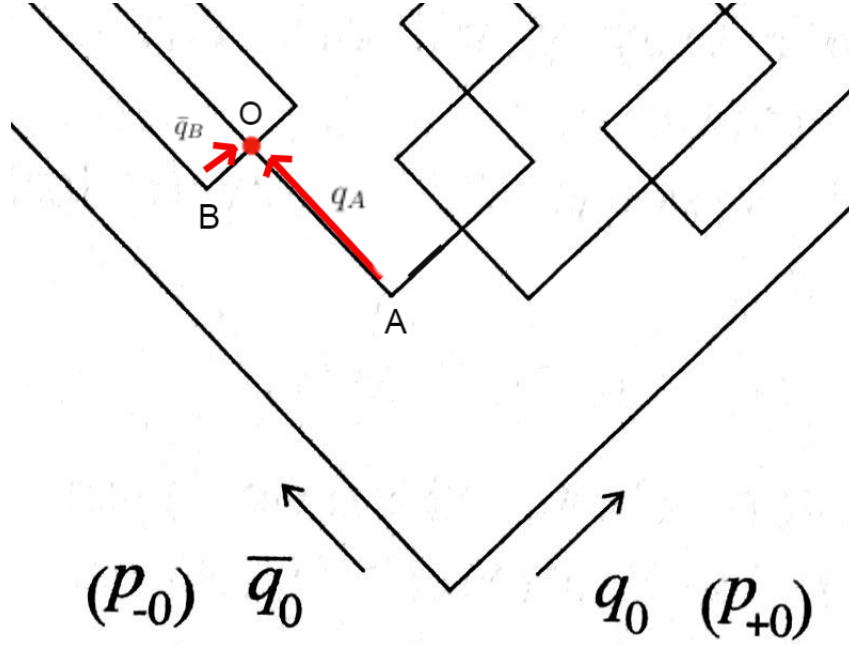


Figure 7: Light cone diagram of single string fragment.

Let q_A be created at vertex $A = (x_A, t_A)$, \bar{q}_B be created at vertex $B = (x_B, t_B)$ with the two quarks meeting at point $O = (x_O, t_O)$. According to eq.(4) and eq.(9), the energy and momentum of each quark is given by:

$$p_A = \kappa(t_A - t_O), p_B = \kappa(t_O - t_B), \quad (15)$$

$$E_A = \kappa(x_A - x_O), E_B = \kappa(x_O - x_B). \quad (16)$$

The total energy and momentum of the $q_A \bar{q}_B$ state is:

$$p = p_A + p_B = \kappa(t_A - t_B), \quad (17)$$

$$E = E_A + E_B = \kappa(x_A - x_B). \quad (18)$$

Since this state corresponds to the Yoyo mode of a meson, it must follow eq.(10):

$$m^2 = E^2 - p^2 = \kappa^2[(x_A - x_B)^2 - (t_A - t_B)^2]. \quad (19)$$

According to this equation, the mass of the resultant meson will only be real (positive) if the distance between the vertices A and B is spacelike. This implies the two vertices cannot be causally connected; in other words, information cannot be shared between them.

In fact, this result can be generalised to all vertices due to the fact that the Lund model framework is Lorentz invariant. In figure 7, the string break at vertex A appears to happen before the string break at vertex B. However, it is a property of Lorentz boosts that we can always find a frame in which one event appears to take place before another. If we

boost to a frame in which vertex B occurs first in time, then the same reasoning that led to eq.(19) can be repeated in this frame, since the physics of the Lund model is unchanged under Lorentz boosts. The A and B subscripts would be switched around in that case in eq.(19).

Therefore, the spacelike separation must hold between *all* vertices, no matter what order they appear to occur in any given frame. Conceptually, the causal disconnect between vertices means that there is nothing special about any particular vertex. They all perform the same function, and their space-time location in a specific frame does not affect the overall output of the string fragmentation process. This will allow us to treat all vertices equally when it comes to calculating useful quantities from the Lund model. Importantly, this also allows us the freedom to pick the order in which we will consider the vertices, without needing to time order them.

3.2 The Schwinger Mechanism

The event of a string break as it has been explained thus far is somewhat arbitrary. An unstable string state can fragment in any number of ways, with the only condition being that the energy of the $q\bar{q}$ pair exceeds that of a stable hadron. In order to quantify the process of string breaks, a further quantum mechanical framework needs to be invoked. The relevant idea is called the Schwinger model, borrowed from quantum electrodynamics (QED). Within QED, it is possible for virtual electron-positron pairs to be created out of quantum fluctuations of the vacuum in the presence of a strong electric field [22]. The Schwinger mechanism by which these virtual particles can be created involves quantum mechanical tunnelling, with a corresponding Gaussian probability distribution [23].

The Lund model assumes that quark-antiquark pairs can be created with the same probability distribution as that of the electron-positron pairs in QED. A string break therefore occurs with a Gaussian probability distribution given by [24]:

$$P(m^2, p_{\perp}^2) = \exp\left(-\frac{\pi m^2}{\kappa}\right) \exp\left(-\frac{\pi p_{\perp}^2}{\kappa}\right) \quad (20)$$

m is the mass of the produced quark, while p_T is the transverse momentum “kick” given to the produced quark by the string break. Transverse momentum is the momentum perpendicular to the direction the string is travelling. Conceptually, this equation describes the probability that a quark-antiquark pair will “tunnel out” into a classical region and become real. The production of heavier quarks such as strange and charm quarks is also suppressed, since a higher mass leads to a smaller probability in the above equation. This string break probability is crucial, as we now have a probabilistic model that can tell us what particles to expect at the end of a full fragmentation process, depending on how much energy an original $q\bar{q}$ pair has.

3.3 Hadron Distribution Functions

Based on the string fragmentation model, distributions can be determined for the probability that a hadron is produced with a certain fraction of the total energy and momentum. This is an essential step in developing a model of hadronisation that is actually useful in simulating real particle events. Once we have these distributions, we can iteratively calculate the probability of a hadron being produced at each step of the fragmentation process. It will be easier to do this if we work in hyperbolic space-time coordinates, defined as [19, p.149]:

$$y = \frac{1}{2} \log \frac{x_+}{x_-}, \quad (21)$$

$$\Gamma = \kappa^2 x_+ x_-. \quad (22)$$

Here, $x_{\pm} = t \pm x$ corresponds to light cone space-time. y is then the rapidity, or the hyperbolic angle. Rapidity ranges from negative infinity along the left side of the positive light cone to positive infinity along the right side of the positive light cone, and is equal to zero along the time axis $x = 0$. An important property of rapidity is that it is additive under multiple Lorentz boosts, unlike velocity which asymptotes as a particle approaches the speed of light. Meanwhile, Γ is related to the squared proper time of the vertex, $\tau^2 = x_+ x_- = t^2 - x^2$. Γ is therefore directly proportional to the energy-momentum of an eventual particle. This is because a change in the time at which a vertex/string break occurs will change the available area for a hadron in the light-cone diagram. The change in area corresponds to a change in invariant mass of the hadron according to eq.(14), which is in turn related to the energy-momentum. Visually, hyperbolic coordinates can be depicted like [25]:

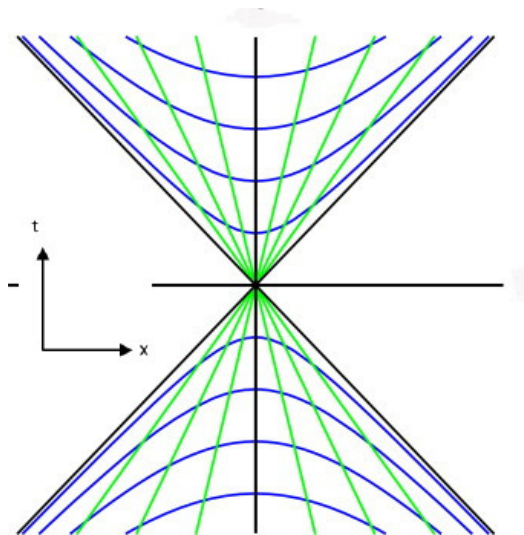


Figure 8: Visual representation of hyperbolic coordinates.

The green lines correspond to constant rapidity, while the blue lines correspond to constant Γ (or, equivalently, constant squared proper time τ^2).

Having made this change of coordinates, we can derive the probability distribution function for a meson to be produced. We first consider an arbitrary stage in a string fragmentation process, where multiple string breaks have occurred. Let us pick two arbitrary vertices that will result in a stable meson between them, as shown below:

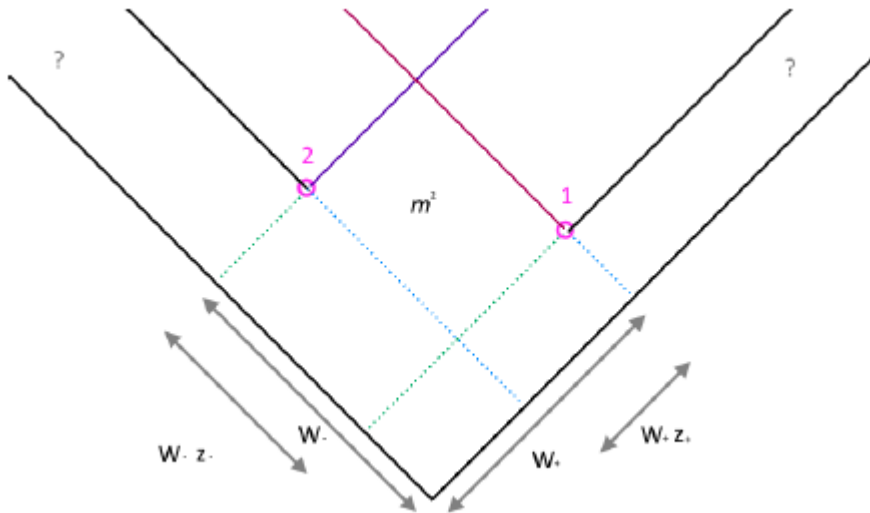


Figure 9: Meson production from two arbitrary vertices.

The initial quark-antiquark pair travel along the light cone with an energy-momentum W_+ and W_- respectively. z_+ and z_- are then the fractions of energy-momentum used from the respective initial energy-momentum to form a meson with invariant mass m^2 . Using these definitions, the hyperbolic coordinate Γ can be written for each vertex:

$$\Gamma_1 = (1 - z_-)W_-W_+, \quad (23)$$

$$\Gamma_2 = (1 - z_+)W_-W_+. \quad (24)$$

The mass squared can also be written using the area of the rectangle labelled by m^2 in figure 9:

$$m^2 = (z_-W_-)(z_+W_+), \quad (25)$$

Eliminating W_{\pm} :

$$\Gamma_1 = \frac{m^2(1 - z_-)}{z_+z_-}, \quad (26)$$

$$\Gamma_2 = \frac{m^2(1 - z_+)}{z_+z_-}. \quad (27)$$

There are now two probabilities that need to be introduced. First, there is the probability of reaching vertex 1 with energy-momentum W_+ , given by $H(\Gamma_1)d\Gamma_1dy_1$. In order for this

probability to be Lorentz invariant, the distribution H must not depend on rapidity y_1 , since it is not a Lorentz invariant quantity. Second, there is the probability of the meson being produced by using the energy-momentum fraction z_+ . This is given by $f(z_+)dz_+$. These two events are independent; z_+ is just a ratio, it does not depend on how much energy is available in the form of W_+ .

The overall probability of a meson being produced with a given energy fraction z_+ at a certain proper time Γ_1 is therefore given by multiplying the probabilities of these two events occurring:

$$H(\Gamma_1)d\Gamma_1dy_1f(z_+)dz_+, \quad (28)$$

A similar equation is obtained for the second vertex by applying the same reasoning:

$$H(\Gamma_2)d\Gamma_2dy_2f(z_-)dz_-. \quad (29)$$

This is exactly the useful quantity we want to obtain from the Lund string model as a whole. If we know the distributions H and f , we can calculate the probability that a given meson will be produced.

A full derivation of the distributions H and f is provided in appendix A. These are the forms of the distributions we obtain:

$$H(\Gamma) = C\Gamma^a \exp(-b\Gamma) \quad (30)$$

$$f(z) = N\frac{1}{z}(1-z)^a \exp\left(\frac{-bm^2}{z}\right) \quad (31)$$

These distributions depend on two parameters a and b , which can be determined experimentally, while N and C are normalisation constants. Since our choice of vertices at the beginning was entirely arbitrary, the same form of the probability will apply to all vertices. We now have an exact form for the distributions $H(\Gamma)$ and $f(z)$, which together provide the probability of a meson being produced at a certain time with a certain energy-momentum fraction, using eq.(28). This allows us to iteratively calculate the probability of a hadron being produced at each step of the hadronisation process. $H(\Gamma)$ and $f(z)$ form the basis for Monte Carlo event generators such as PYTHIA to numerically simulate hadronisation, and are enshrined within the code contained in such programs. This is a realisation of the aim of the Lund string model to non-perturbatively describe the overall process of hadronisation.

4 Thermal String Tension

Having described the normal formulation of the Lund model, we can begin the process of modifying it. This will be performed by introducing a time-dependent thermal string tension instead of the usual constant κ . Before making this significant adjustment, we will describe why we have made this change in the first place.

4.1 Motivation

There have long been speculations about the existence of a thermal component in the hadronisation stage. From decades-old electron-positron collisions at LEP, it is possible to obtain particle multiplicities that have a reasonable fit to a thermal form. Specifically, the particle multiplicities appear to closely resemble a Boltzmann distribution at a temperature T [27].

Another piece of evidence is the discovery of a “ridge” of enhanced particle production around the azimuthal angle of trigger jets in proton-proton collisions at the ATLAS detector [28]. This ridge had previously only been seen in heavy-ion collisions, where it is due to the formation of a quark-gluon plasma [29]. A quark-gluon plasma is a thermal object, so its potential presence in proton-proton collisions points to the possible existence of a temperature of some kind. The standard Lund model has no explanation for the thermal features seen in these experiments, suggesting it is inadequate in its current state to describe the entirety of hadronisation.

There are further theoretical arguments for why a thermal element could be relevant within the Lund model. Berges, Floerchinger and Venugopalan have argued that the ordinary Lund conception of a string ignores the fact that different QCD string regions are necessarily entangled [30]. Within the density matrix formalism of quantum information, one can define a reduced density matrix for a region A by performing a trace over the Hilbert space corresponding to another region B [31]:

$$\rho_A = \text{Tr}_B \rho \quad (32)$$

Here, ρ corresponds to the mixed quantum state of the two string regions. The entanglement entropy is then defined as the Von Neumann entropy associated with region A:

$$S_A = -\text{Tr}[\rho_A \ln \rho_A] \quad (33)$$

Entanglement entropy is a measure of the entanglement between two regions [32]. In the same way as a statistical mechanical system can define a temperature associated with its entropy, a temperature can be defined corresponding to the entropy between two entangled regions. Therefore, by ignoring entanglement, the standard Lund model is also ignoring any associated thermal effects. Berges, Floerchinger and Venugopalan go on to show that the entanglement entropy between regions of the QCD string has a temperature that depends inversely on proper time, $T = \frac{1}{2\pi\tau}$. The proper time is defined here in hyperbolic coordinates, corresponding to the blue lines in figure 8. In other words, the string has a high temperature to begin with, which cools off as time goes on. This thermal dependence on proper time will be very important when it comes to defining a thermal string tension.

The central claim of this thesis is that the temperature associated with the entanglement of quarks linked by a string can be modelled as an increase in the string tension of the normal Lund model, so that κ is no longer a constant. In order to justify this step, a more detailed description of the QCD vacuum is required, in the context of superconductivity. A simple traditional electromagnetic superconductor consists of loosely bound states of two

electrons, called "Cooper pairs." An external applied magnetic field will induce a supercurrent of Cooper pairs in a material according to Lenz's law, such that an induced magnetic field is created in the superconducting medium that opposes the external field [19].

There exist two different types of electromagnetic superconductors, type I and type II. The classification of a superconductor is based on two parameters: ξ , the spatial extent of the Cooper pair states; and λ , the penetration depth of the external magnetic field in opposition to the induced magnetic field [33]. For type I superconductors, $\xi \gg \lambda$ and neither the Cooper pairs nor the applied magnetic field can move to the area between the superconducting state and the rest of the material. The superconducting state will then try to minimise these boundary regions, condensing the field energy into a spherical shape since a sphere has the smallest ratio of boundary-to volume. If the Cooper pairs are stretched longitudinally, then a cylindrical "flux tube" minimises the boundary area of the field. For type II superconductors, $\lambda \gg \xi$ and there exists no restriction on where the magnetic field and Cooper pairs can populate within the material. For a critical range of external magnetic field strength, the superconducting material is punctuated by a series of vortices that each carry a single quantum of magnetic flux, $\Phi_0 = \frac{h}{2e}$.

In QCD, the vacuum is taken to behave analogously to a superconducting material, where the colour field is the equivalent of the electromagnetic field and quark-antiquark pairs replace Cooper pairs. However, the sizes of ξ and λ of the superconducting QCD vacuum are not currently determinable a priori, leaving it on the borderline between type I and type II [34]. If the QCD vacuum is a type II superconductor, then we can obtain a physical interpretation of the string described in the Lund model. The ends of the vortices are usually treated as monopoles exerting a force proportional to a quantum of magnetic flux, in the same way as in the electromagnetic case [35]. This force is then a potential physical description of the string tension, and the medium that is "heating up" due to entanglement is in fact the QCD vacuum itself. There have been no studies performed either experimentally or theoretically to investigate the dependence of this force on temperature, since the exact microdynamics of superconductors remain difficult to pin down [36]. However, it does not appear incoherent to state that the presence of a temperature will increase the force associated with flux/vortex lines, thereby increasing the string tension.

This argument is not intended as a definitive proof that thermal effects will affect the string tension of the Lund model, rather it is an attempt to describe a conceivable way in which the existence of a temperature might change the standard conception of strings in the context of hadronisation. There are other possible ways in which a temperature could be incorporated into the Lund model, such as through thermal fluctuations in the string tension [37]. However such a model does not introduce an explicit dependence on temperature, and as such it lacks a physical explanation of the thermal effects in terms of entanglement entropy. One could also argue that the existence of a temperature will mean that the string no longer follows the same simple motion of the Lund model, requiring a complete reformulation of the string's mechanics. Perhaps it is no longer meaningful in such a thermal context to speak of a string at all. Before entertaining this possibility, it is worth pointing out that the Lund model has seen decades of success in predicting a plethora of experimental results. The few thermal

features that are unaccounted for should not necessarily motivate a complete overhaul of the model, it seems more likely that there is a small effect that is not currently taken into account. An increased string tension that depends on temperature is able to incorporate such a thermal effect, without undermining the structure of a model that provides largely correct experimental predictions.

4.2 Description

A simple general form can now be postulated for the new temperature-dependent string tension κ_{therm} :

$$\kappa_{therm} = \kappa_0 + \alpha T \tag{34}$$

κ_0 refers to the zero-temperature constant string tension, T is the temperature and α is an unknown constant to be determined. Borrowing from the definition of temperature provided by Berges, Floerchinger and Venugopalan, we state that the temperature in fact depends on the proper time, according to $T = \frac{1}{2\pi\tau}$. Substituting the expression for the temperature into the above equation:

$$\kappa_{therm} = \kappa_0 + \frac{\alpha}{2\pi\tau} \tag{35}$$

This expression diverges as $\tau \rightarrow 0$, however we expect perturbative QCD to apply at those very early times anyway. In order to regulate this divergence, we introduce a constant τ_0 :

$$\kappa_{therm} = \kappa_0 + \frac{A}{\tau + \tau_0} \tag{36}$$

As $\tau \rightarrow 0$, $\kappa_{therm} \rightarrow \kappa_0 + \frac{A}{\tau_0}$ which is a constant defining the maximum string tension. This is the form of the thermal tension that will be used, giving us two free parameters built into the model. A plot is shown below of the thermal string tension as a function of proper time compared to the zero-temperature string tension:

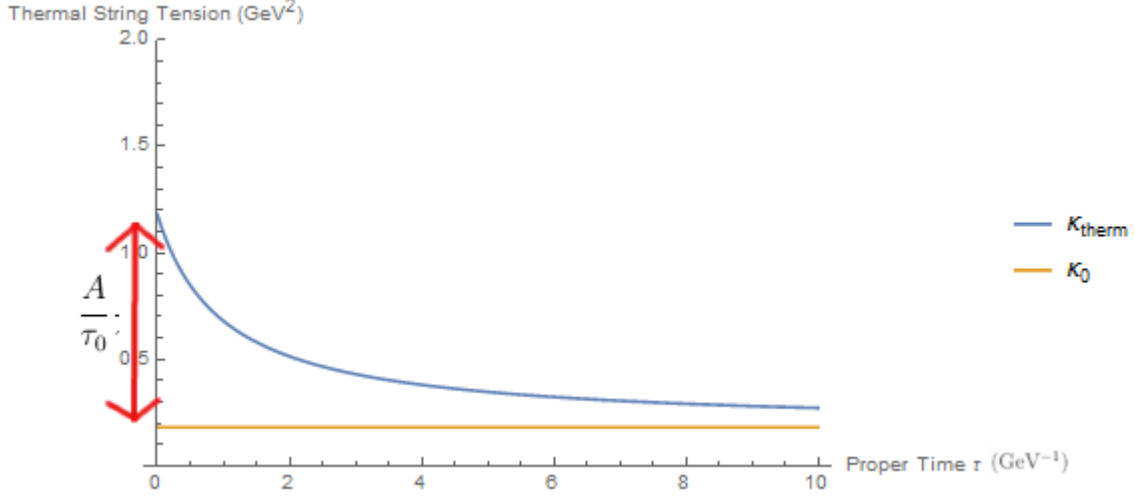


Figure 10: Form of thermal string tension compared to normal tension as a function of proper time for $\tau_0 = 1$, $A = 1$.

The thermal tension reduces to the constant $\kappa_0 = 0.18 \text{ GeV}^2$ at late times, while the maximum tension $\frac{A}{\tau_0}$ occurs at $\tau = 0$.

To check if this is a reasonable form for the tension, we can calculate the potential by solving the differential eq.(3). This means integrating the tension with respect to the spatial coordinate x , in the same way as for eq.(9). This is not as simple as multiplying all the terms in κ_{therm} by x as in eq(9), since τ is itself a function of x , $\tau = \sqrt{t^2 - x^2}$. The full solution to the differential equation is:

$$E(x) = E_0 + \kappa_0 x + \frac{\tau_0 \arctan\left(\frac{x}{\sqrt{-t^2 + \tau_0^2}}\right)}{\sqrt{-t^2 + \tau_0^2}} - \frac{\tau_0 \arctan\left(\frac{\tau_0 x}{\sqrt{-t^2 + \tau_0^2} \sqrt{t^2 - x^2}}\right)}{\sqrt{-t^2 + \tau_0^2}} - \arctan\left(\frac{x \sqrt{t^2 - x^2}}{-t^2 + x^2}\right) \quad (37)$$

While this complicated equation might appear on the surface to be an undesirable form for the potential, plotting it against x for several values of time (not proper time) reveals a linear form:

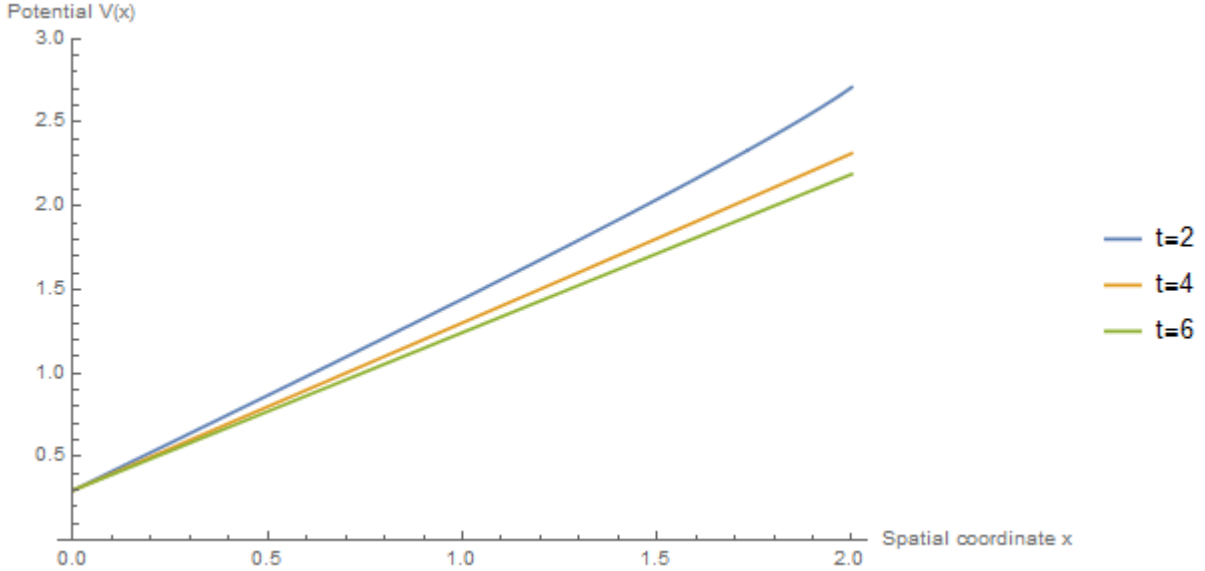


Figure 11: Form of potential as a function of x -coordinate at different values of time for $\tau_0 = 1$, $A = 1$, $E_0 = 0.3$.

Thus, the linear form of the potential is retained under the new thermal string tension, in accordance with figure 1 from lattice QCD. The presence of the temporal component t acts to change the gradient of the potential slightly, but since lattice QCD calculations are static by design they would not be sensitive to such a variation. The lattice actually does see a steeper gradient at small separations anyway, ascribed to the Coulomb part of the potential below 0.5 fm in figure 1, which is neglected in the standard Lund model. The fact that the potential is linear with respect to the x coordinate is enough to suggest that our introduction of a thermal string tension is not implausible.

4.3 Effects

Having motivated and described the thermal string tension, we can now investigate what changes will be made to string fragmentation. It is assumed that the mechanics of the string motion remain the same, and that the means by which a string can fragment is still via the Schwinger mechanism. It is further assumed that vertices remain causally disconnected, so that we can treat all vertices equally as in the normal Lund model. There is a clear problem with this assertion. It was claimed in section 5.1 that string regions are entangled, and so it would seem that any vertex produced from a string would have to carry some shared information. As such, vertices cannot truly be causally disconnected. This argument is valid, but we will continue with our assumption nonetheless. It should be pointed out that the usual Lund model ignores this aspect of entanglement as well, and by invoking a thermal string tension we are taking more entanglement effects into account than the normal model does. Furthermore, it is unclear how a causal connection between vertices would affect string fragmentation, if at all.

In addition, even if we ignore entanglement, vertices do in some sense still have shared information. Conservation of energy and momentum means that particles are sensitive to the energies and momenta of other particles, implying that there is some overall information transfer that must be taking place. Any effects this causal connection has are likely small, and so it is a perfectly reasonable approximation to treat particles as causally disconnected. We will make the same approximation in ignoring any entanglement effects on causal disconnection. Any information sharing from overall energy and momentum conservation is ignored in the normal Lund model as well.

Crucially, the form of this new string tension retains the Lorentz invariance of the original Lund model. The conserved quantity between frames is the area spanned by the string, given by $A = \frac{m^2}{\kappa_{therm}^2}$ after substituting the new tension into eq.(14). Since κ_{therm} depends only on τ , which is unchanged under a Lorentz boost by definition (proof in appendix B), the area will also remain unchanged as before.

Another aspect of string fragmentation that will remain unchanged is the hadron distribution function $f(z)$. $f(z)$ is derived on the basis that the string breaks have already occurred, and has no dependence on κ as a result. The derivation in section 3.3 proceeds in exactly the same way, with the only difference being the definition of Γ in eq.(22):

$$\Gamma = \kappa_{therm}^2 x_+ x_- = \left(\kappa_0 + \frac{A}{\tau + \tau_0} \right)^2 x_+ x_- \quad (38)$$

Changing the coordinate Γ in this way means Γ is no longer directly proportional to τ^2 , but the derivation of $f(z)$ never invokes the form of Γ directly. The derivation also never involves any dependence on τ , so a different relationship between Γ and τ should not affect any of the steps in section 3.3.

Given that eqs.(23-27) are unchanged by the presence of a thermal string tension, we can obtain an equation relating the energy-momentum fraction z to τ . By rearranging eq.(25), we have:

$$z_- = \frac{m^2}{z_+ W_- W_+} \quad (39)$$

Substituting into eq.(23):

$$\Gamma_1 = \left(1 - \frac{m^2}{z_+ W_- W_+} \right) W_- W_+ \quad (40)$$

Simplifying:

$$\Gamma_1 = W_- W_+ - \frac{m^2}{z_+} \quad (41)$$

Combining eq.(38) and eq.(41), and using $x_+ x_- = \tau^2$ with $z_+ = z$ since choice of vertex is arbitrary:

$$\left(\kappa_0 + \frac{A}{\tau + \tau_0}\right)^2 \tau^2 = W_- W_+ - \frac{m^2}{z} \quad (42)$$

Now solving for z :

$$z = \frac{m^2}{W_- W_+ - \left(\kappa_0 + \frac{A}{\tau + \tau_0}\right)^2 \tau^2} \quad (43)$$

Plotting z as a function of τ for both zero-temperature and thermal string tension:

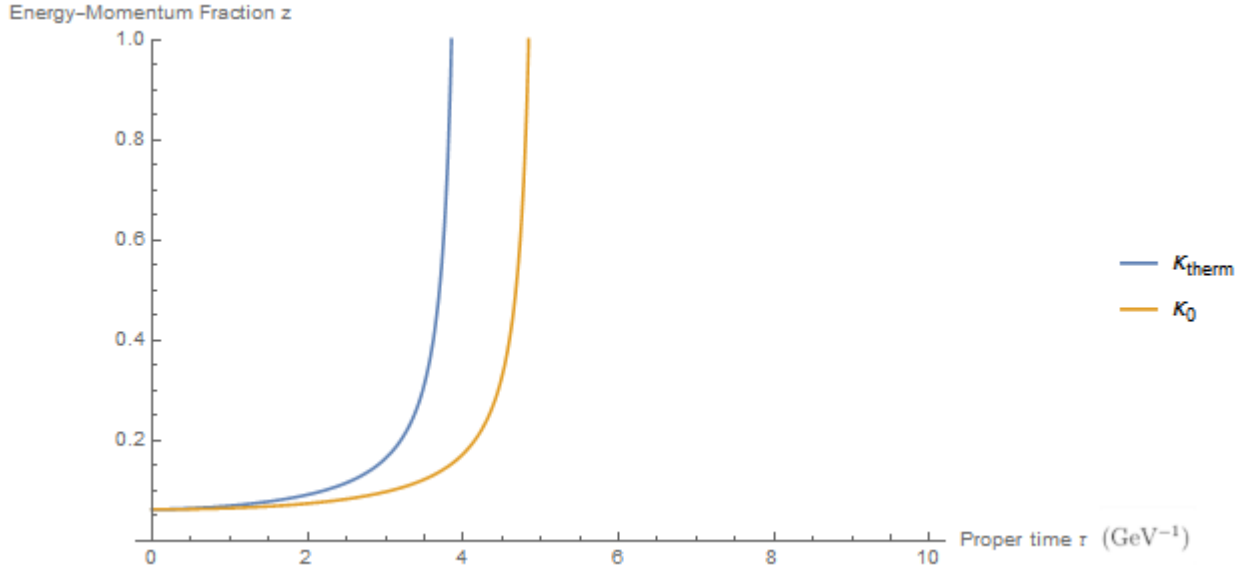


Figure 12: Relationship between z and τ for $A = 1$, $\tau_0 = 1$, $m = 1$ and $W_- = W_+ = 4$.

The above plot demonstrates that the energy-momentum fraction increases to its maximum of 1 (when all the available energy-momentum is taken) at earlier times. This means that an increased string tension results in more energetic hadrons being produced at earlier times. In other words, though the choice of z through $f(z)$ is the same as for the normal Lund model, the time at which z occurs is pushed earlier by a thermal string tension. This result will inform our intuition about what physical effects an enhanced tension has on the string system.

Another effect of the increased string tension is a wider transverse momentum (p_\perp) spectrum for produced quarks. The width σ^2 of the p_\perp spectrum is given by the average value of the p_\perp squared [38]:

$$\sigma^2 = \langle p_\perp^2 \rangle \quad (44)$$

Since the p_\perp is factorised in the Schwinger tunneling probability (eq.(20)), the average value can be written as [1]:

$$\sigma^2 = \langle p_{\perp}^2 \rangle = \frac{\pi}{\kappa_0} \int_0^{\infty} p_{\perp}^2 \exp\left(\frac{-\pi p_{\perp}^2}{\kappa_0}\right) dp_{\perp}^2 \quad (45)$$

Performing this integral, we obtain:

$$\sigma^2 = \frac{\kappa_0}{\pi} \quad (46)$$

The width σ^2 will therefore increase under an increased string tension κ_{therm} . It should be noted that this is the width of the quark p_{\perp} spectrum, since the Schwinger mechanism only describes the p_{\perp} of quarks produced from a single string break. The hadrons will receive p_{\perp} kicks from two quarks corresponding to two breakups, and so the actual width will be twice as large.

The mass factor in the Schwinger probability also contains the string tension, and so the probability of producing a quark with a given mass will change as well:

$$P(m^2) \propto \exp\left(-\frac{\pi m^2}{\kappa_0}\right) \quad (47)$$

This change in $P(m^2)$ will manifest as a change in the ratio of strange quarks to up/down quarks, since this ratio is given by:

$$P(s : u/d) = \frac{P(m_s^2)}{P(m_{u/d}^2)} = \frac{\exp\left(-\frac{\pi m_s^2}{\kappa_0}\right)}{\exp\left(-\frac{\pi m_{u/d}^2}{\kappa_0}\right)} \quad (48)$$

Where m_s is the mass of the strange quark and $m_{u/d}$ is the mass of the up/down quarks, taken to be roughly the same here since we only care about the ratio to the strange quark. It is known from experimental data that there is a general suppression of strange quark production compared to up and down quarks, with a strangeness ratio of around 0.2-0.3 [39]. Under an increased string tension, the ratio becomes:

$$P'(s : u/d) = \exp\left(-\frac{(m_s^2 - m_{u/d}^2)}{\kappa_{therm}}\right) \quad (49)$$

Defining $\Delta m^2 = m_s^2 - m_{u/d}^2$ and writing in terms of κ_0 :

$$P'(s : u/d) = \exp\left(-\frac{\Delta m^2}{\kappa_0} \frac{\kappa_0}{\kappa_{therm}}\right) \quad (50)$$

Substituting eq.(48):

$$P'(s : u/d) = P(s : u/d)^{\frac{\kappa_0}{\kappa_{therm}}} \quad (51)$$

An increased string tension therefore corresponds to decreasing the power $\frac{\kappa_0}{\kappa_{therm}}$, which in turn increases $P'(s : u/d)$ since $P(s : u/d)$ is a ratio (less than 1). We therefore expect there to be an increased number of strange particles to up and down quarks in this thermal string model compared to the Lund model.

5 Implementation in PYTHIA

Having described the anticipated changes to be made to the Lund model, these results can now be implemented in PYTHIA, a C++ Monte Carlo event generator used to simulate particle collisions. Before doing so, it will be worth defining new free parameters that have more physical meaning than A and τ_0 . A is currently arbitrary, acting as a dilation factor in eq.(36), while τ_0 translates the tension so as to avoid any divergence at $\tau = 0$. τ_0 must have the same units as τ , since they are being added together in a denominator. Since $\tau^2 = t^2 - x^2$, and in natural units $[t] = [x] = \text{GeV}^{-1}$, the units of τ and τ_0 must be GeV^{-1} . The overall units of the second term in κ_{therm} must have the same units as κ_0 , which means it must be in either GeV^2 or GeV/fm depending on which units are chosen for the string tension. The units of A will therefore be GeV or fm^{-1} given that the units of the denominator are GeV^{-1} .

Although we know the units of A and τ_0 , it is not obvious how to interpret them physically, particularly the free parameter A . We will therefore reparameterise the string tension, beginning by multiplying the second term in κ_{therm} by $\frac{\tau_0}{\tau_0} = 1$:

$$\kappa_{therm} = \kappa_0 + \frac{A}{\tau_0} \frac{\tau_0}{\tau + \tau_0} \quad (52)$$

The factor $\frac{A}{\tau_0}$ has some physical significance. It defines the maximum size of κ_{therm} , when $\tau = 0$, as shown in figure 10. The maximum value of the thermal tension is given by the y -intercept, $\kappa_{max} = \kappa_0 + \frac{A}{\tau_0}$. Let $\Delta\kappa_{max} = \frac{A}{\tau_0} = \kappa_{max} - \kappa_0$. $\Delta\kappa_{max}$ will be one of the new free parameters, with units of $[\kappa_0] = \text{GeV}^2$ or GeV/fm . $\Delta\kappa_{max}$ will therefore define the size of the difference in string tension at maximum temperature compared to zero temperature.

In order to obtain a meaningful alternative to τ_0 , we will introduce another new parameter $k = \frac{\tau_0}{\langle \tau \rangle}$, where $\langle \tau \rangle$ is the average value for τ . Since τ_0 has the same units as τ , this will mean k is a dimensionless quantity. In making this modification, the average value for τ will have to be determined somehow. This will be done by brute force calculation in the next section. The reparameterised form of the string tension can now be stated by substituting in the new free parameters:

$$\kappa_{therm} = \kappa_0 + \Delta\kappa_{max} \frac{k \langle \tau \rangle}{\tau + k \langle \tau \rangle} \quad (53)$$

5.1 Veto Algorithms

PYTHIA contains a default settings database, which can be freely and easily altered by initialising the main program with different settings. Within this database is the constant `StringFlav:ProbStoUD = 0.217`, which defines the ratio of strange quark production to up/down quark production from string breaks. There is also the variable `StringPT:sigma = 0.335`, which defines the width of the p_\perp spectrum of produced hadrons. It might therefore seem that all we need to do is increase these two constants in accordance with the increased string tension to encapsulate the thermal effects of the new model. However, it is inappropriate to introduce a global modification for these variables. In our model, the string tension depends on τ , the proper time at which a vertex occurs, and this varies for each

produced hadron. Since the strangeness production ratio and p_{\perp} spectrum width depend on κ_{therm} , they will also be different for each hadron. We therefore need a way of changing these parameters on a case-by-case basis, rather than imposing a blanket value for all hadrons.

The changes to the Lund model have been implemented in the form of a `UserHook`. A `UserHook` is a piece of functionality within PYTHIA that allows a user to intervene at various stages of a particle event and perform certain operations. By using a `UserHook`, we don't necessarily have to alter the source code of PYTHIA, and we can step in part-way through the hadroniation process and make our changes on an individual basis. The `UserHook` that will be utilised is called Modified Hadronization, and it contains multiple useful methods. The first method is called `doChangeFragPar`, which allows the user to change any relevant parameters before the string fragmentation is performed. We could therefore change `StringFlav:ProbStoUD` and `StringPT:sigma` to be whatever we want. However, the implementation of `doChangeFragPar` means that in order to change these parameters, the relevant settings need to be reinitialised with the modified values. If we wanted to use this method in this way, then we would need to reinitialise for every single string in every event, which is very inefficient since we eventually want to build up statistics of many events. This leaves us with the `doVetoFragmentation` method, which gives us information about the current hadron about to be produced and allows us to choose whether we want to accept or reject it. If we reject it, then PYTHIA will continue generating trial hadrons for us, until we eventually decide not to veto.

Both `UserHooks` have access to the Γ of the vertex within the `StringEnd` class, from which we can calculate τ using eq.(38):

$$\Gamma = \left(\kappa_0 + \Delta\kappa_{max} \frac{k < \tau >}{\tau + k < \tau >} \right)^2 \tau^2 \quad (54)$$

Once we know τ we can then calculate the modified string tension κ_{therm} . It should be pointed out that Γ is calculated within PYTHIA by using z in eq.(41), the energy-momentum fraction. z is in turn calculated from the standard Lund fragmentation formula, eq.(31). This demonstrates the importance of $f(z)$ remaining unchanged under a thermal string tension. If it was not, more significant changes to the process by which strings are fragmented in PYTHIA would be required.

Solving for τ gives a complicated form (negative and non-real solutions are discarded):

$$\tau = \frac{1}{2} \left(\frac{\sqrt{\Gamma}}{\kappa_0} - k < \tau > - \frac{\Delta\kappa_{max} k < \tau >}{\kappa_0} \right) + \frac{1}{2} \sqrt{\frac{\Gamma}{\kappa_0^2} - \frac{2\Delta\kappa_{max}\sqrt{\Gamma}k < \tau >}{\kappa_0^2} + \frac{\Delta\kappa_{max}^2 k^2 < \tau >^2}{\kappa_0^2} + \frac{2\Delta\kappa_{max} k^2 < \tau >^2}{\kappa_0}} \quad (55)$$

As long as we have some way of calculating τ from Γ , it doesn't matter how complex the relationship between them is, we have all the necessary information.

At this point we can also calculate in PYTHIA the average proper time of a vertex, $\langle \tau \rangle$. We replace κ_{therm} in eq.(54) with the default κ_0 , which gives a much simpler equation for τ :

$$\tau = \frac{\sqrt{\Gamma_0}}{\kappa_0} \quad (56)$$

We then use the above equation to find τ in a `UserHook` with nothing changed from baseline PYTHIA. By looping over many events, adding up the total τ and then dividing by the number of times the `UserHook` was called, the average τ can be calculated by brute force. After 1,000,000 events, $\langle \tau \rangle$ was found to be equal to 1.2152 GeV^{-1} . This value will be used in the string tension from now on.

Since `doVetoFragmentation` does not allow us to directly change any parameters, we will need some way of altering the string fragmentation process only through vetos. The Veto Algorithm will provide the mathematical basis for us to do exactly that. It is used in different forms in a variety of contexts, such as emission probabilities in parton showers, where it is called the Sudakov Veto Algorithm [40]. For a given trial probability \hat{P} , the Veto Algorithm states that in order to obtain an actual probability of P , we accept with a probability of [41]:

$$P_{accept} = \frac{P}{\hat{P}} \quad (57)$$

In our context, the trial strangeness ratio or p_\perp spectrum can be identified as \hat{P} , and P is the actual strangeness ratio or p_\perp spectrum that we want. The accept probability that we put into `doVetoFragmentation` will then be equal to the ratio of P to \hat{P} . In this way, we can change the string fragmentation parameters while avoiding having to reinitialise constantly with `doChangeFragPar`.

5.2 Strangeness Ratio

First, let us determine the accept probability for an enhanced strangeness ratio which we will implement in `doVetoFragmentation`. The ratio of strange to up/down quarks is ordinarily given by the trial probability of obtaining a strange quark divided by the trial probability of obtaining an up/down quark:

$$P(s : u/d) = \frac{\hat{P}_s}{\hat{P}_{u/d}} \quad (58)$$

Since we always accept whatever quark we are given normally, the trial probabilities are equal to the actual probabilities. However, the new probabilities after the potential for a veto are given by:

$$P'(s : u/d) = \frac{P_s}{P_{u/d}} \quad (59)$$

Here, $P_s \neq \hat{P}_s$, and $P_{u/d} \neq \hat{P}_{u/d}$, since we are not necessarily accepting the trial quark we were given. We will first calculate the probability of obtaining an up/down quark, then the

probability of obtaining a strange quark, before dividing them to find the new strangeness ratio according to the above equation.

$P_{u/d}$ is equal to the probability of getting an up/down trial quark times the probability of accepting it, plus the probability that the up/down quark was rejected but the next trial quark was up/down and was accepted, plus the probability that the second up/down quark was rejected but the third trial quark was up/down, and so on. $P_{u/d}$ is in fact an infinite series:

$$P_{u/d} = \hat{P}_{u/d}P_{accept} + \hat{P}_{u/d}P_{reject}(\hat{P}_{u/d}P_{accept} + \hat{P}_{u/d}P_{reject}(\hat{P}_{u/d}P_{accept} + \hat{P}_{u/d}P_{reject}(\dots \quad (60)$$

Given that we want to primarily study the effects of an increased strangeness ratio, we assume that all trial strange quarks are accepted (in principle one could include a probability to reject \hat{P}_s , in which case there would be additional terms in the above equation corresponding to the cases where we reject a trial strange quark and accept the next up/down quark). Since $P_{reject} = 1 - P_{accept}$:

$$P_{u/d} = \hat{P}_{u/d}P_{accept} + \hat{P}_{u/d}(1 - P_{accept})(\hat{P}_{u/d}P_{accept} + \hat{P}_{u/d}(1 - P_{accept})(\dots \quad (61)$$

Expanding first bracket:

$$P_{u/d} = \hat{P}_{u/d}P_{accept} + \hat{P}_{u/d}^2P_{accept}(1 - P_{accept}) + \hat{P}_{u/d}(1 - P_{accept})(\hat{P}_{u/d}P_{accept} + \hat{P}_{u/d}(1 - P_{accept})(\dots \quad (62)$$

Further expansions will lead to an infinite sum:

$$P_{u/d} = \hat{P}_{u/d}P_{accept} + \hat{P}_{u/d}^2P_{accept}(1 - P_{accept}) + \hat{P}_{u/d}^3P_{accept}(1 - P_{accept})^2 + \dots \quad (63)$$

Factorising:

$$P_{u/d} = \hat{P}_{u/d}P_{accept}(1 + \hat{P}_{u/d}(1 - P_{accept}) + \hat{P}_{u/d}^2(1 - P_{accept})^2 + \dots) \quad (64)$$

Using the sum of an infinite geometric series:

$$P_{u/d} = \hat{P}_{u/d}P_{accept} \left(\frac{1}{1 - \hat{P}_{u/d}(1 - P_{accept})} \right) \quad (65)$$

This is the probability of obtaining an up or down quark, the denominator in eq.(59). Now we need to find P_s in order to determine the eventual accept probability that we want to implement in PYTHIA. The probability of obtaining a strange quark has a slightly simpler form, since strange quarks are always accepted, however we still need to take into account the possibility of an up/down quark being rejected and then a strange quark being accepted:

$$P_s = \hat{P}_s + \hat{P}_{u/d}(1 - P_{accept})(\hat{P}_s + \hat{P}_{u/d}(1 - P_{accept})(\dots \quad (66)$$

Expanding and then factorising in the same way as for $P_{u/d}$:

$$P_s = \hat{P}_s(1 + \hat{P}_{u/d}(1 - P_{accept}) + \hat{P}_{u/d}^2(1 - P_{accept})^2 + \dots) \quad (67)$$

$$P_s = \hat{P}_s \left(\frac{1}{1 - \hat{P}_{u/d}(1 - P_{accept})} \right) \quad (68)$$

Now that we have $P_{u/d}$ and P_s , we can find the new strangeness ratio by substituting them into eq.(59):

$$P'(s : u/d) = \frac{P_s}{P_{u/d}} = \frac{\hat{P}_s \left(\frac{1}{1 - \hat{P}_{u/d}(1 - P_{accept})} \right)}{\hat{P}_{u/d} P_{accept} \left(\frac{1}{1 - \hat{P}_{u/d}(1 - P_{accept})} \right)} \quad (69)$$

$$P'(s : u/d) = \frac{\hat{P}_s}{\hat{P}_{u/d} P_{accept}} \quad (70)$$

We know the form of the modified probability in terms of κ_{therm} from eq.(51):

$$P'(s : u/d) = P(s : u/d)^{\frac{\kappa_0}{\kappa_{therm}}} = \frac{\hat{P}_s}{\hat{P}_{u/d} P_{accept}} \quad (71)$$

Solving for the accept probability:

$$P_{accept} = \frac{\hat{P}_s}{\hat{P}_{u/d} P(s : u/d)^{\frac{\kappa_0}{\kappa_{therm}}}} \quad (72)$$

Since $\frac{\hat{P}_s}{\hat{P}_{u/d}}$ is equal to the original strangeness ratio in eq.(58):

$$P_{accept} = \frac{P(s : u/d)}{P(s : u/d)^{\frac{\kappa_0}{\kappa_{therm}}}} = P(s : u/d)^{1 - \frac{\kappa_0}{\kappa_{therm}}} \quad (73)$$

This is the probability for us to accept a given quark which will be implemented in PYTHIA. Since the the normal strangeness ratio $P(s : u/d)$ and the normal string tension κ_0 are constants, we can calculate the probability for the quark to be accepted by substituting in the trial values for \hat{P}_s , $\hat{P}_{u/d}$, and the calculated value for κ_{therm} based on the τ of the vertex. The veto probability will then be $1 - P_{accept}$.

5.3 Transverse Momentum

We can also develop an accept probability for trial p_\perp spectra. This will be more complicated, since the trial p_\perp can take on a range of values instead of a single value. A standard two-dimensional Gaussian probability distribution in momentum is given by:

$$P(p_x, p_y) = \frac{1}{\pi\sigma^2} \exp\left(\frac{-p_x^2 - p_y^2}{\sigma^2}\right) \quad (74)$$

p_x and p_y take on values from $-\infty$ to ∞ , and in its current state this Gaussian is normalised to 1. The change of variables $p_x = p_\perp \cos(\phi)$ and $p_y = p_\perp \sin(\phi)$ will allow us to write the Gaussian in terms of p_\perp . Since this is a conversion to cylindrical coordinates, an

additional Jacobian factor of p_{\perp} is needed when integrating with respect to p_{\perp} and ϕ , so the form of the Gaussian becomes:

$$P(p_{\perp}, \phi) = \frac{p_{\perp}}{\pi\sigma^2} \exp\left(\frac{-p_{\perp}^2}{\sigma^2}\right) \quad (75)$$

Integrating with respect to ϕ gives additional factor of 2π since the Gaussian has no dependence on ϕ :

$$P(p_{\perp}) = \frac{2p_{\perp}}{\sigma^2} \exp\left(\frac{-p_{\perp}^2}{\sigma^2}\right) \quad (76)$$

From eq.(46), $\sigma^2 = \frac{\kappa_0}{\pi}$, so:

$$P(p_{\perp}) = \frac{2p_{\perp}\pi}{\kappa_0} \exp\left(\frac{-\pi p_{\perp}^2}{\kappa_0}\right) \quad (77)$$

This Gaussian matches the Schwinger probability, but is now properly normalised to 1 as required for a probability distribution function. Since $p_{\perp}^2 = p_x^2 + p_y^2$, p_{\perp} takes on values between 0 and ∞ . The above Gaussian is the trial p_{\perp} spectrum ordinarily generated by PYTHIA. The new Gaussian under a thermal string tension will be given by:

$$P'(p_{\perp}) = \frac{2p_{\perp}\pi}{\kappa_{therm}} \exp\left(\frac{-\pi p_{\perp}^2}{\kappa_{therm}}\right) \quad (78)$$

A plot of the new Gaussian for different values of κ_{therm} is shown below, to illustrate the broadening of the p_{\perp} spectrum under an increased tension:

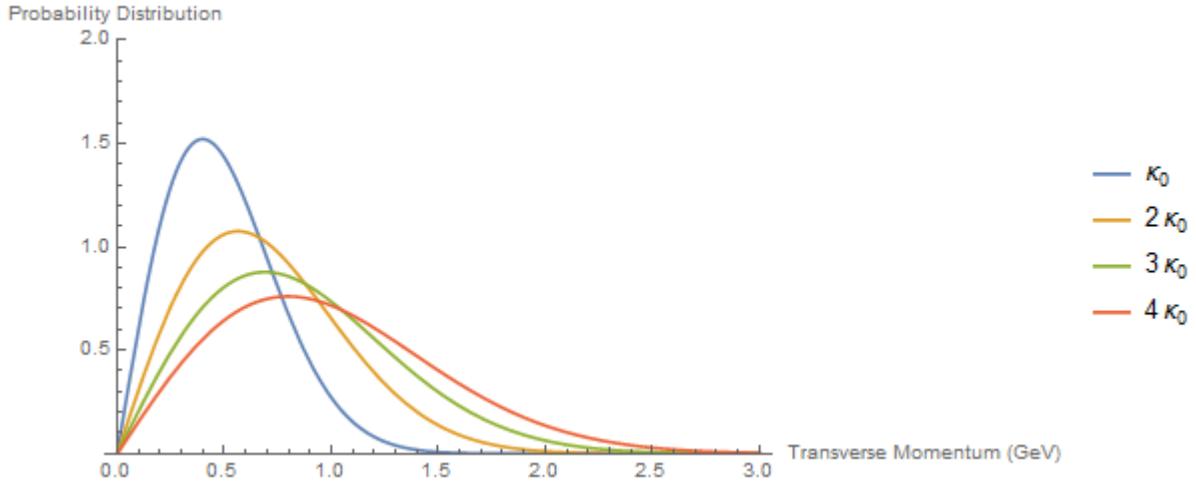


Figure 13: Change in p_{\perp} spectrum with increasing thermal string tension.

The Veto Algorithm states that the accept probability should be given by the ratio of the new Gaussian to the old trial Gaussian:

$$P_{accept} = \frac{P'(p_{\perp})}{P(p_{\perp})} \quad (79)$$

We can then implement this accept probability by calculating κ_{therm} for each hadron, and substituting it into the new Gaussian $P'(p_{\perp})$. We also need to calculate the old Gaussian using the normal value for κ_0 , so that we can divide the two Gaussians.

We obviously also need access to the trial p_{\perp} of the hadron as generated by PYTHIA in order to make these calculations. One must be very careful when picking this p_{\perp} , since it depends heavily on which frame one chooses. The transverse momentum that has been discussed thus far is taken to be defined in the frame of the string. In the lab frame, the transverse momentum would need to be modified by a Lorentz boost, and the relevant p_{\perp} would no longer be given by $p_x^2 + p_y^2$. PYTHIA provides easy access to the p_{\perp} in the lab frame through the event record, which keeps track of all the particles and their properties at any given point in the event. Instead of using the lab frame p_{\perp} in the event record, we will use the `pxHad` and `pyHad` variables taken from the `StringEnd` class, which we have access to in the `UserHooks`. p_x and p_y will then be in the string frame, allowing us to calculate the p_{\perp} using $p_x^2 + p_y^2$.

There is, however, a clear problem with the accept probability for a trial p_{\perp} as it is currently formulated. At some point, the broader p_{\perp} distribution will be greater than the original distribution, resulting in an accept probability that is greater than 1. In other words, the accept probability will only be usable for p_{\perp} values less than the intersection points in figure 14. We could address this problem by simply setting the probability to be equal to 1 if the modified distribution is larger than the unchanged distribution. However this means we cannot sample the entire modified p_{\perp} distribution (for further discussion see appendix C).

A possible solution is to increase the amplitude of the original Gaussian distribution, so that the intersection point is pushed higher and more of the spectrum is sampled. This could be done with an equation like:

$$P_{accept} = \frac{1}{N} \frac{P'(p_{\perp})}{P(p_{\perp})} \quad (80)$$

By increasing N , the size of the trial Gaussian will be increased. The accept probability will then be less than 1 for higher p_{\perp} values, meaning fewer data points will be blindly accepted. There is an issue with this as well, as can be seen by plotting the accept probability again but for different values of N :

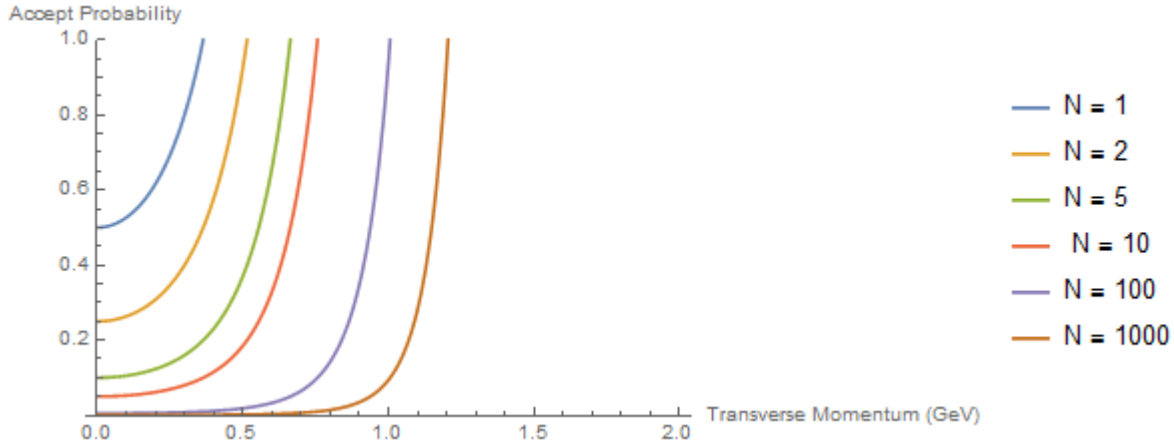


Figure 14: Form of accept probability for different values of N , at a string tension of $2\kappa_0$.

We find that in order to push the accept probability to incorporate higher values of p_\perp , we require N to grow almost exponentially. The probability to accept p_\perp less than 1 GeV can be seen to decrease to almost zero in the above plot as N is increased to 1000. At the same time, the trial distribution is giving us p_\perp values that are mostly in this region, as can be seen in figure 15. As such, we will be rejecting almost all particles that are given to us, except for the very few that happen to fall in the range where the probability is substantial. This means our efficiency is reduced enormously, since we have to continue generating trial hadrons until we finally get one with a high enough accept probability. It can also be seen that as N is increased, the form of the accept probability tends more and more towards a vertical line. This means we are effectively not sampling any p_\perp values below this peak, which was what we were trying to avoid in the first place.

We will therefore return to the `doChangeFragPar` method, in which we can reinitialise the `StringPT:sigma` with an enhanced p_\perp width. While this is an inefficient method, it is still much more efficient than using a high value of N , and this way we can be sure that we are sampling the whole modified distribution. We will keep the veto algorithm for the strangeness ratio, since it means we don't also have to reinitialise a second time with a new `ProbStoUD` as well.

6 Results

The following results were generated by simulating electron-positron collisions at 91 GeV that annihilate to produce a Z boson, which then decays to a single quark-antiquark pair. This allows us to study the simplest case of a single string stretched between two quarks. A copy of the `UserHook` code used to modify the hadronisation process is in appendix D. Each data point corresponds to 10,000 events.

6.1 Proof of Concept

We will first consider the results of our modifications in an ideal case, where the quark-antiquark pair are produced directly along the z axis. This is not a realistic scenario, but it will help give us an understanding of the effects we would expect to observe if we knew exactly what axis to measure the transverse momentum with respect to. We will later study the case where we don't know what direction the quarks are produced along, requiring us to approximate the necessary axis as experimentalists do. We will also turn off hadron decay and final state radiation, again to simplify the situation.

As an initial check, we can plot the average p_{\perp} and strangeness ratio as a function of the free parameters to make sure they are increasing as expected. The average p_{\perp} is determined by averaging over the p_{\perp} of all produced hadrons, while the strangeness ratio is calculated by adding up all the accepted quarks in the string fragmentation process for each flavour, and then dividing the number of strange quarks by the number of up/down quarks. If we first plot the average p_{\perp} as a function of $\Delta\kappa_{max}$:

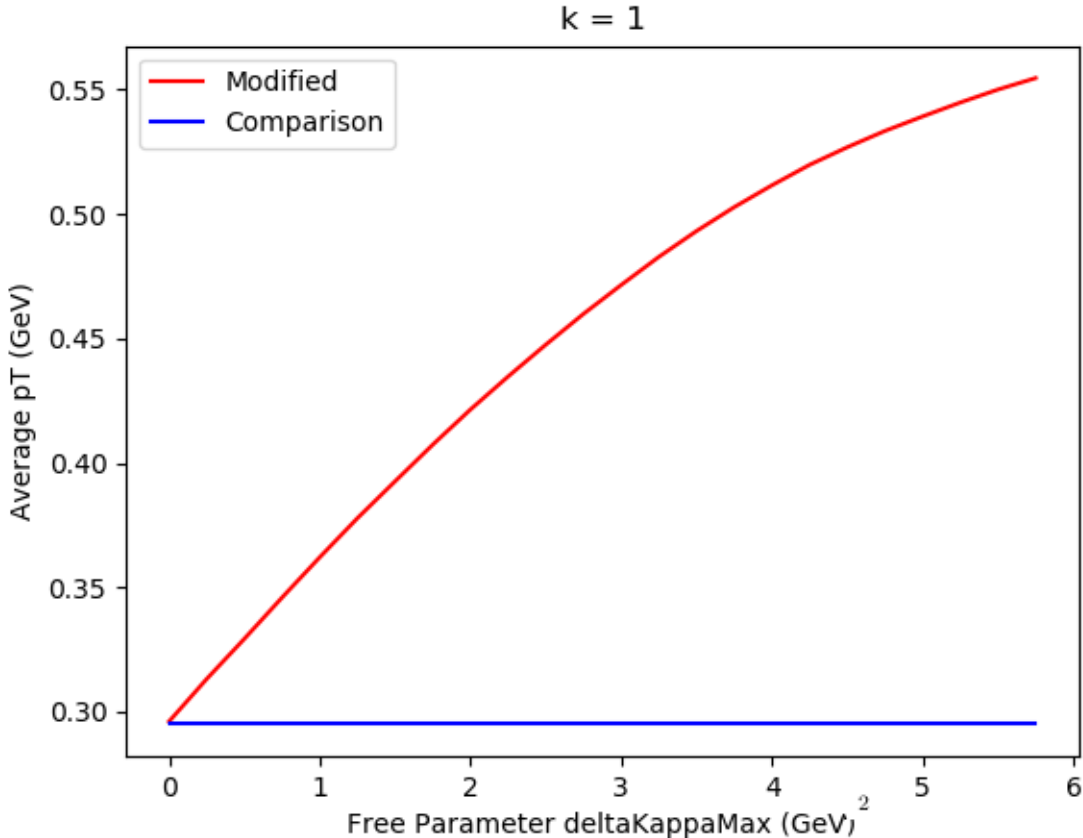


Figure 15: Change in average p_{\perp} as a function of $\Delta\kappa_{max}$ at $k = 1$ compared to baseline PYTHIA value.

The values chosen for $\Delta\kappa_{max}$ range between 0 and 6 GeV², in increments of 0.25 GeV²,

which will be maintained across all future plots as well. This range is chosen since it covers small enhancements to the string tension all the way to massive enhancements. The usual value for κ_0 is 0.18 GeV^2 , so a value of $\Delta\kappa_{max} = 1 \text{ GeV}^2$ is already a sizeable increase to the string tension. If $k = 1$ and τ takes on its average value of 1.2152 GeV^{-1} , then according to eq.(53) the enhanced string tension is equal to 0.5 GeV^2 , which is nearly three times the baseline value. We extend the range for $\Delta\kappa_{max}$ up to 6 GeV^2 , since beyond that value the string tension becomes so high that the accept probability in eq.(73) is very small, and the efficiency is drastically reduced. At that point we are effectively only accepting strange quarks anyway, so extending $\Delta\kappa_{max}$ further is unlikely to give us much more new information. At $\Delta\kappa_{max} = 6 \text{ GeV}^2$, the string tension is also so energetic that we can question whether we are even considering an entirely non-perturbative system anymore. We therefore only include these higher values for the sake of completeness, and to see what happens to the model when it is taken to an extreme.

It can be seen that an increased $\Delta\kappa_{max}$, corresponding to an increased thermal string tension, results in an increased average p_{\perp} as expected. The size of the difference is substantial at this stage, with the average p_{\perp} approaching nearly twice the zero temperature value at high $\Delta\kappa_{max}$. It is also clear that the new model reduces to the original Lund model when $\Delta\kappa_{max}$ is set to zero, at which point the average p_{\perp} is the same in both cases. The relationship between the two variables appears approximately linear, before leveling off as $\Delta\kappa_{max}$ reaches very large values. An explanation for this levelling off effect is that there is only so much energy available in the event to be given to the p_{\perp} . As a result, the p_{\perp} cannot be increased indefinitely by increasing the string tension. In order to check if this is a valid explanation, we can plot the average p_{\perp} again with twice the centre of mass energy of the previous plot (182 GeV):

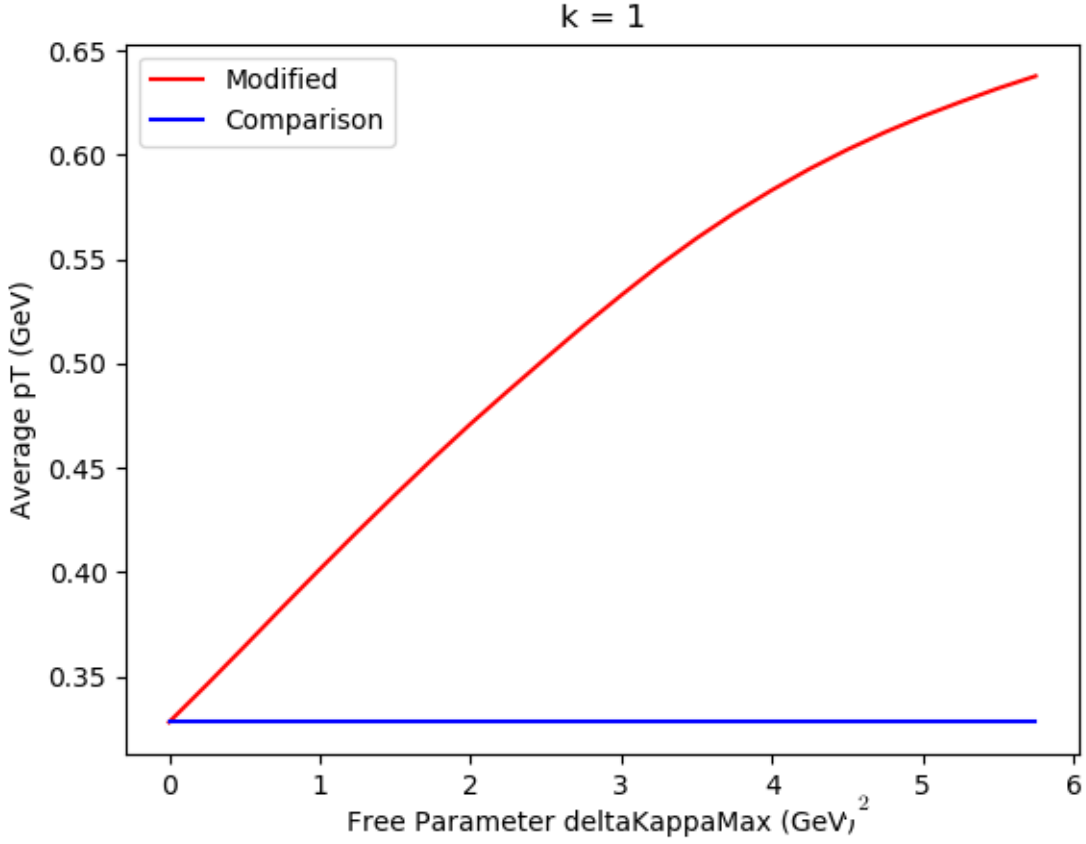


Figure 16: Change in average p_{\perp} as a function of $\Delta\kappa_{max}$ at $k = 1$ for 182 GeV.

Compared to the previous plot, the average p_{\perp} reaches a higher value and the linear shape is retained for slightly longer. This suggests that the levelling off of the average p_{\perp} is a phase space effect, and if we increased the centre of mass energy far enough then the p_{\perp} would effectively increase indefinitely with the string tension.

Another reason why increasing the centre of mass energy would increase the average p_{\perp} is that it minimises the endpoint effects of the string. When the initial quark-antiquark pair are produced from the hard process decay of the Z boson, they have zero p_{\perp} . It is only the quarks produced from string breaks via the Schwinger mechanism that receive any p_{\perp} kicks. By increasing the centre of mass energy, more string breaks occur, and there are more particles with non-zero p_{\perp} to offset the original endpoint quarks with zero p_{\perp} . On average, therefore, the p_{\perp} will increase.

It is also worth plotting the average p_{\perp} as a function of the other free parameter k :

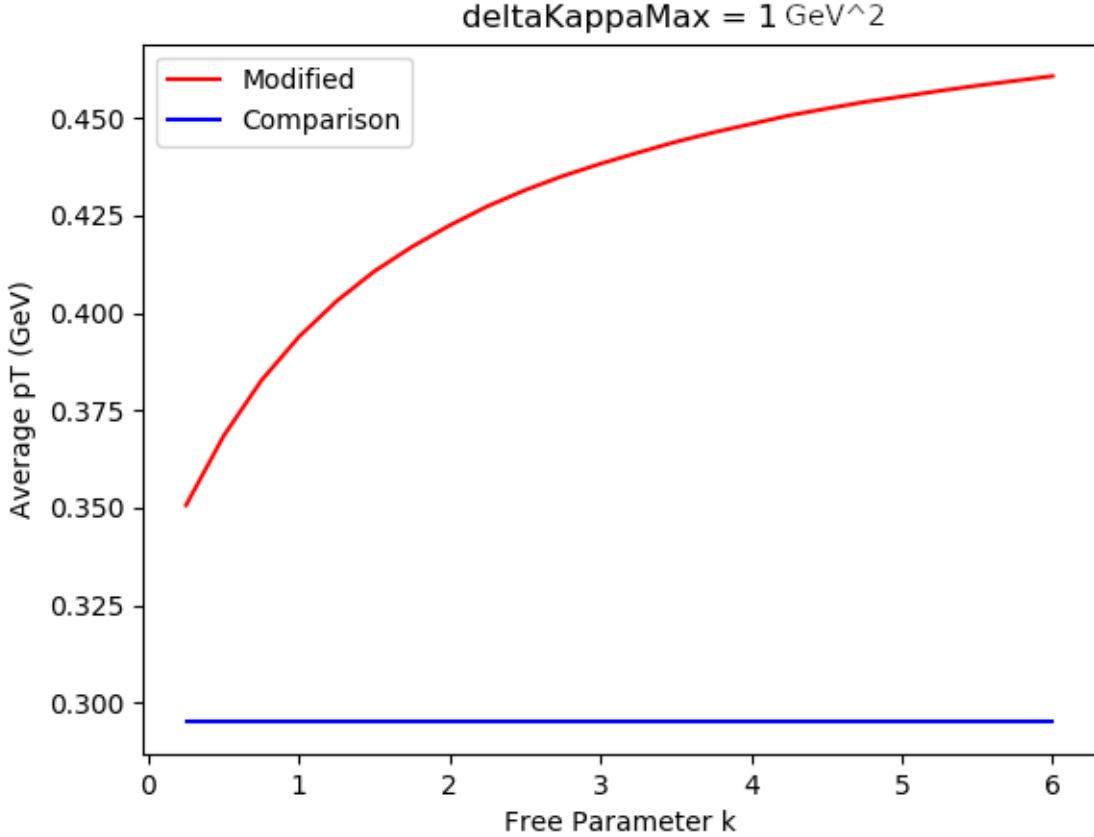


Figure 17: Change in average p_{\perp} as a function of k at $\Delta\kappa_{max} = 1$ compared to baseline PYTHIA.

It is apparent that increasing k also increases the average p_{\perp} somewhat, though it begins to level off at lower values than that of $\Delta\kappa_{max}$. If we revisit the form of the thermal string tension in eq.(53), it is clear that increasing k will increase the fraction $\frac{k\langle\tau\rangle}{\tau+k\langle\tau\rangle}$ towards a value of 1, if τ is held constant. For example, at $\tau = \langle\tau\rangle$, the fraction becomes $\frac{k}{1+k}$, so increasing k will cause this term to get closer to 1. In other words, increasing k will cause the overall string tension to increase towards $\kappa_{therm} = \kappa_0 + \Delta\kappa_{max}$. We would therefore expect the thermal string tension to asymptote as k becomes large, and since p_{\perp} depends linearly on the string tension when $\Delta\kappa_{max} = 1$, the p_{\perp} should also asymptote as we have observed. Small values of k will not reproduce the zero temperature value of average p_{\perp} , since the presence of a non-zero $\Delta\kappa_{max}$ means the tension will still be enhanced.

We will hold k at a constant value for the rest of these results. This is partly for the sake of brevity, to avoid presenting twice as many plots. We also primarily want to examine here the dependence of various quantities on the size of the string tension, which is already encapsulated by $\Delta\kappa_{max}$. It may nevertheless be worth considering variations in k in future work. k is correlated with the time-dependence of the thermal string tension, so there may be some additional interesting information captured by this free parameter.

Now the strangeness ratio can be plotted as a function of $\Delta\kappa_{max}$:

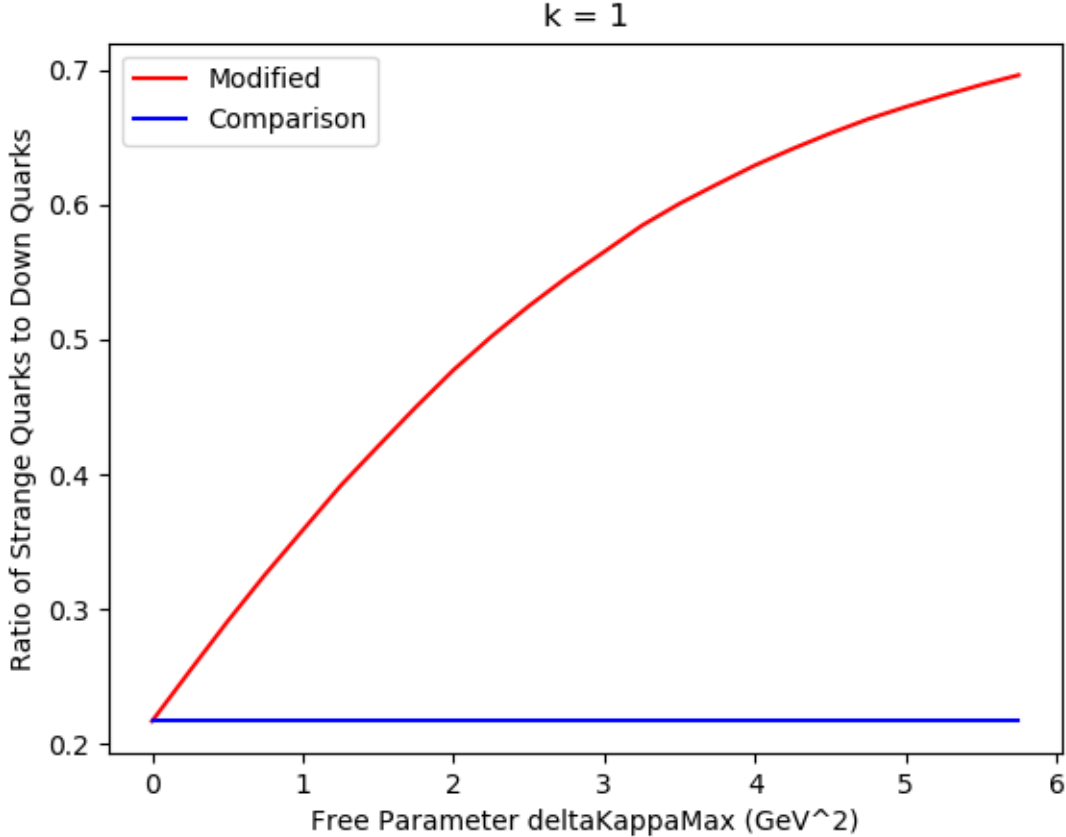


Figure 18: Change in strangeness ratio as a function of $\Delta\kappa_{max}$ compared to baseline PYTHIA.

The strangeness ratio is here taken as the ratio of strange to down quarks accepted, but it could equally be taken as the ratio of strange to up quarks. The ratio is seen to increase as expected, with the baseline value of 0.217 recovered at $\Delta\kappa_{max} = 0$. The ratio again flattens out, due to there only being so much energy available to convert into the heavier strange quarks compared to up and down quarks. The centre of mass energy can be increased again to increase the strangeness ratio further, as in the case of average p_{\perp} .

So far we've seen that the presence of a thermal string tension results in an increased amount of strange hadrons, as well as an increased average p_{\perp} . A natural next step would be to predict that strange hadrons in particular are receiving more p_{\perp} than hadrons without any strange content. If found, this would demonstrate a link between average p_{\perp} and strangeness. Such a link would be an interesting prediction of the model by itself, given that there exists no current analysis of electron-positron collisions that investigates the dependence of p_{\perp} on hadrons with specifically strange content. If such an analysis were performed, the theoretical results of our model could potentially be observed. There does exist experimental evidence

that a link between p_{\perp} and strangeness is possible. In proton-proton collisions at the RHIC (Relativistic Heavy Ion Collider), an analysis of average p_{\perp} for different hadron types was performed, yielding the following plot [42, 43]:

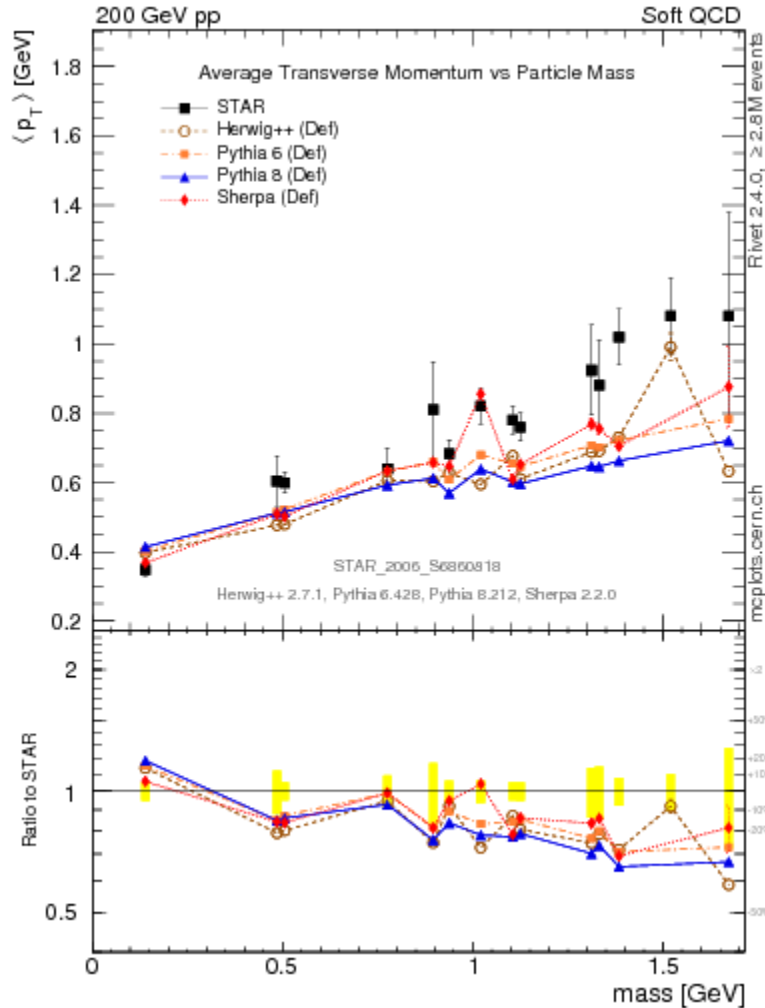


Figure 19: Average p_{\perp} as a function of particle mass in proton-proton collisions.

The first data point corresponds to the average p_{\perp} of pions, the second point to kaons and the third to rho mesons. The key point here is that the data (black points) is well described by PYTHIA (blue points) for pions and rho mesons, whereas the kaons appear to have more p_{\perp} than is predicted. A difference between these types of mesons is the fact that pions and rho mesons have no strange content, whereas kaons contain a strange quark. This suggests a possible connection between strangeness and enhanced p_{\perp} , even in proton-proton collisions which are much more complicated than electron-positron collisions.

In order to test if our model predicts that strange hadrons have more p_{\perp} than non-strange hadrons, the ratio of different hadron average p_{\perp} to pion average p_{\perp} was calculated as a function of $\Delta\kappa_{max}$. This will tell us how the average p_{\perp} of different types of hadrons

varies compared to the average p_{\perp} of pions under a thermal string tension. Various different strange mesons were chosen for this analysis, along with both charged and neutral pions and rho mesons as a point of comparison. Positively and negatively charged particles were grouped together and labelled with just a positive sign. On this basis, the following plot was generated:

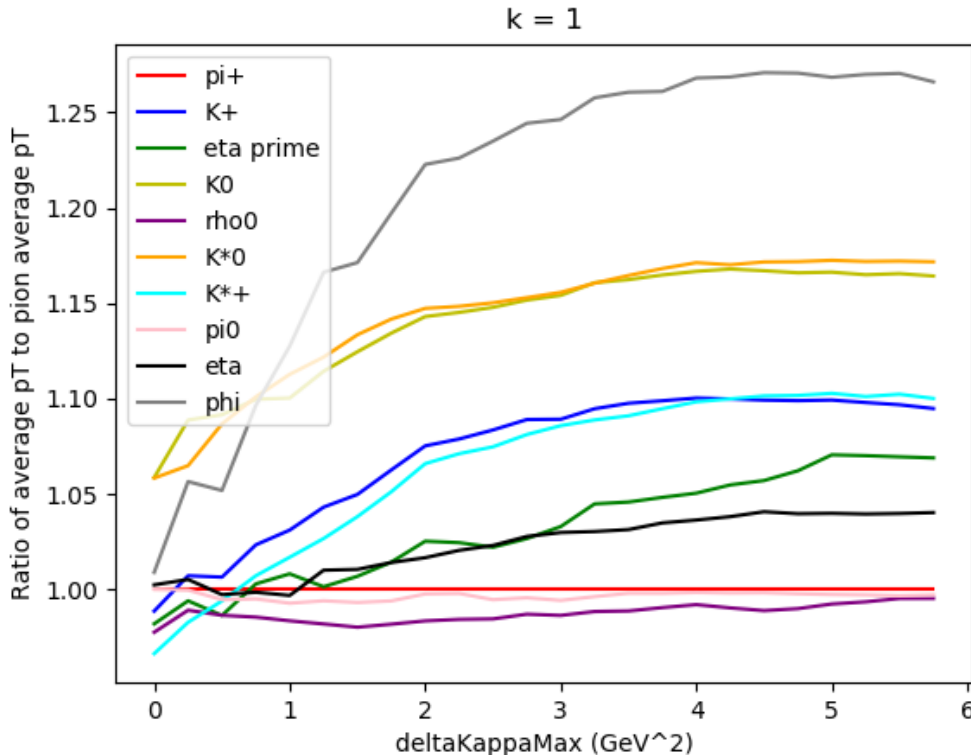


Figure 20: Average p_{\perp} ratio to pions as a function of $\Delta\kappa_{max}$ for different meson types.

All the particles with strange content (K^0 , K^+ , K^{*0} , K^{*+} , η , η' , ϕ) can be seen to have an increased average p_{\perp} relative to the pions, compared to their zero-temperature values. This difference grows as $\Delta\kappa_{max}$ increases. In particular, the ϕ meson consists of two strange quarks, and has the largest p_{\perp} enhancement of any of the particles considered here, more than 25% at its peak. The kaon average p_{\perp} is moderately enhanced, since they all contain one strange quark. The η and η' mesons both have a slightly enhanced p_{\perp} , since they only have a strange quark some of the time. The p_{\perp} of the ρ meson (no strangeness) increases only slightly, if at all, which demonstrates a stark difference between the p_{\perp} of hadrons with and without strange content.

A point of concern might be the difference between the average p_{\perp} for charged and uncharged kaons, which is present with the enhanced string tension turned off at $\Delta\kappa_{max} = 0$ and is consistent across all values of $\Delta\kappa_{max}$. On the face of it, there is no reason why there should be this difference, since a charged kaon differs by an uncharged kaon only by picking up an up quark rather than a down quark. Since our model of hadronisation treats up and

down quarks equally, it seems very unlikely that this difference is due to a modification we have made.

A plausible explanation is that there is an asymmetry in the production of up and down quarks from the hard process Z decay. As explained earlier in this section, initial quarks produced from the hard process have zero p_{\perp} . If more up quarks are produced from the Z decay than down quarks, then the p_{\perp} of any resulting kaons that pick up an up quark (charged) will be lower than for any kaons that pick up a down quark (uncharged). Since this is an effect of the endpoints of the string, we can again increase the centre of mass energy to minimise the effects of the hard process, expecting that the difference between charged and uncharged kaons should be reduced. This is indeed what we see when the centre of mass energy is doubled:

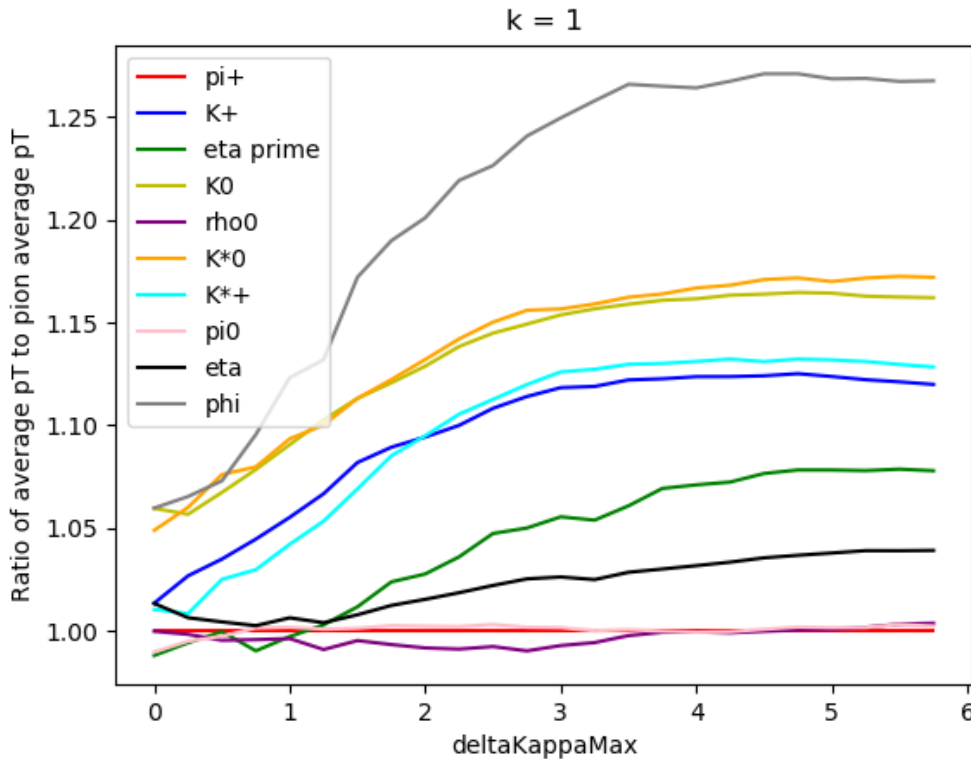


Figure 21: Average p_{\perp} ratio to pions as a function of $\Delta\kappa_{max}$ for different meson types at 182 GeV.

The initial difference between charged and uncharged kaons is smaller at zero temperature compared to the previous plot at 91 GeV, and remains so for non-zero values of $\Delta\kappa_{max}$. The difference is therefore most likely due to endpoint quarks. This is an interesting feature of the model, since it allows us to observe any endpoint effects, or instead study the hadrons created purely from fragmentation by simply increasing the centre of mass.

We might wonder at this point how it is possible for there to be more average p_{\perp} as well

as more heavy strange particles, both of which require more energy, given that there is the same amount of centre of mass energy available. We seem to be getting more energy for free, which is impossible. The answer to this problem is that there are actually fewer particles being produced per event. This is a problem, since particle multiplicity per event is a well measured quantity that is closely reproduced by the baseline parameters within PYTHIA [43, 44]. In order to restore the number of particles back to the original amount, we can tune the input values of `StringFlav:ProbStoUD` and `StringPT:sigma` to be lower than normal when we are first initialised in PYTHIA. This will partially offset the increase in strangeness and p_{\perp} , while increasing the number of particles. We can see this effect in the below plot of particle number as a function of the tuned value for `StringPT:sigma`:

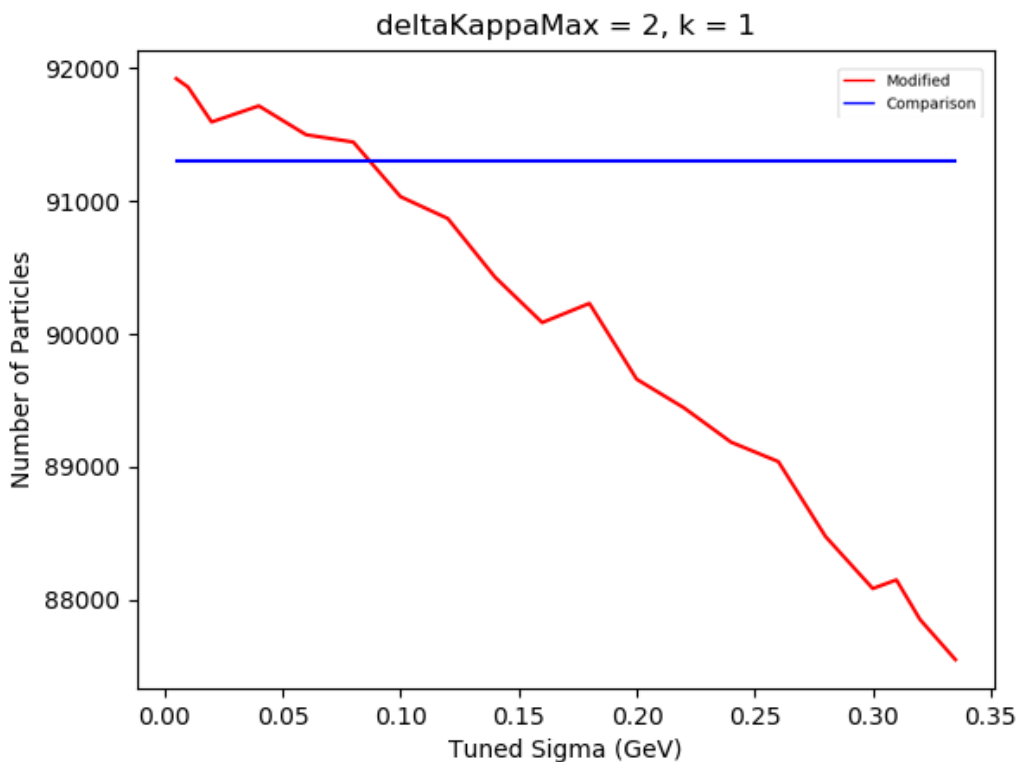


Figure 22: Number of particles in 10000 events as a function of tuned p_{\perp} spectrum width, at $k = 1$ and $\Delta\kappa_{max} = 2$.

This plot shows that the number of particles is significantly lower at the usual value of `StringPT:sigma` = 0.335 GeV when the thermal string tension is in effect compared to when it is not. Decreasing `StringPT:sigma` increases the number of particles back to its original number.

If we want to always have the same number of particles per event under our thermal string tension, then we would need to tune `StringFlav:ProbStoUD` and `StringPT:sigma` like this for every value of the free parameters we choose. This is too time-consuming, since

it would involve manually observing the number of particles without the thermal string tension turned on, then tuning until the number of particles is roughly the same after turning the thermal tension on, and repeating for every $\Delta\kappa_{max}$, and then repeating the whole process again for every set of results we want to study. Instead, we will tune for just a few values of $\Delta\kappa_{max}$, to see what effect it is having specifically on the relationship between strangeness and p_{\perp} in figure 20. This was done by decreasing the values of `StringFlav:ProbStoUD` and `StringPT:sigma` until the total number of particles was within 1% of the original number of particles with no enhanced tension. We also turned on hadron decays and final state radiation, in order to obtain the most realistic total number of particles. It should be noted that for values of $\Delta\kappa_{max}$ between 0 and 0.5, there is no need to tune at all, since the number of particles does not differ by more than 1%.

After performing this tuning procedure, the following plot was generated:

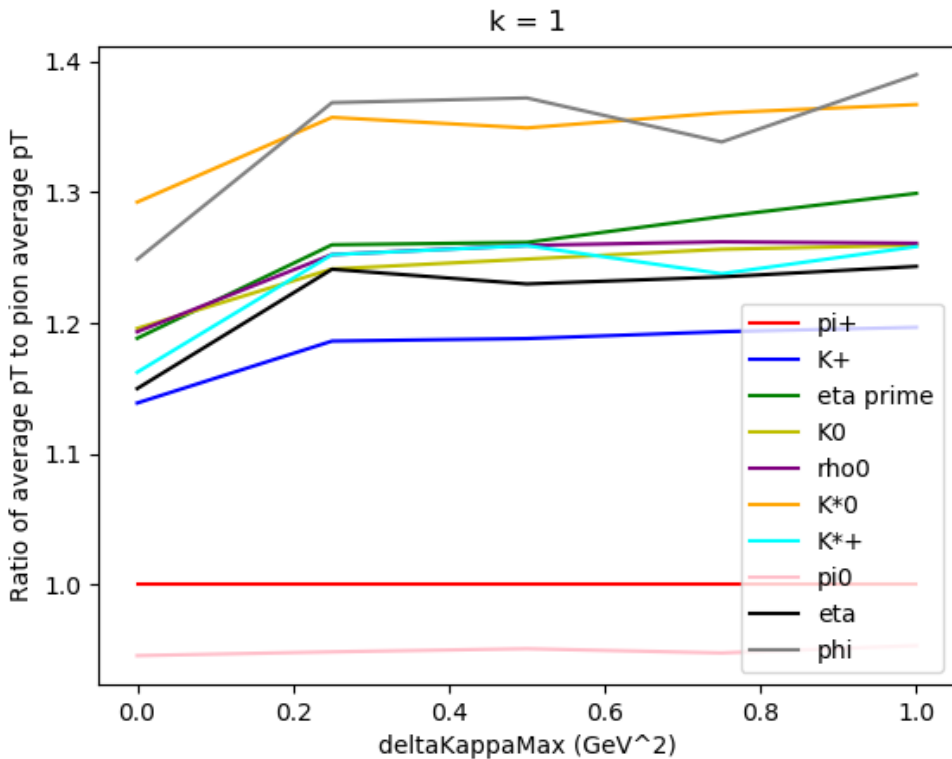


Figure 23: Average p_{\perp} ratio to pions as a function of $\Delta\kappa_{max}$ for different mesons after tuning.

The starting ratio for each meson may look slightly different than in figures 20 and 21. This is due to the fact that hadrons are being allowed to decay here, which can obviously result in different types of particles being produced with different momenta. The key observation is that after an initial increase in average p_{\perp} for the strange mesons compared to the pions, the ratio then starts to flatten out as the tuning kicks in around 0.5 GeV^2 . This indicates that if we want to maintain roughly the same number of particles as we had before

introducing the enhanced tension, we will need to accept a significant dampening of the increased strangeness p_{\perp} above $\Delta\kappa_{max} = 0.5 \text{ GeV}^2$.

6.2 A Realistic Analysis

So far we have been investigating the effects of our new model in an ideal case where the string axis coincides with the z axis of the collider. In reality, the quark-antiquark pair can be produced in any direction. This poses a problem for experimentalists in measuring the p_{\perp} of a given particle in an event. They cannot immediately tell what direction the quark-antiquark pair was produced, since the quarks are not measurable directly, and so the p_{\perp} cannot be measured nicely along a predetermined axis. Instead, they have to approximate the direction in which the quarks were most likely produced, based on where they observe measurable particles like hadrons and leptons in their detectors. This is usually done in electron-positron collisions by calculating a *sphericity* axis, or a *thrust* axis, and then measuring the p_{\perp} with respect to that axis. The sphericity axis is defined using a sphericity tensor [45]:

$$S^{\alpha\beta} = \frac{\sum_i p_i^{\alpha} p_i^{\beta}}{\sum_i |\mathbf{p}_i|^2} \quad (81)$$

Here, α and β run over the x , y and z components of the momentum. After diagonalizing this tensor, one can define three eigenvectors with three associated eigenvalues. The sphericity axis then defined as the eigenvector with the largest eigenvalue.

In order to find the thrust axis, a quantity called thrust (T) must be calculated [46]:

$$T = \frac{\sum_i |\mathbf{n} \cdot \mathbf{p}_i|}{\sum_i |\mathbf{p}_i|} \quad (82)$$

The thrust axis is then defined as the vector \mathbf{n} that maximises the quantity T . Thrust has an advantage over sphericity in that it is infrared safe. An infrared safe quantity is insensitive to any physics occurring at low energy [47]. Sphericity is not infrared safe, since it has a dependence on the momentum squared. This means that the sphericity tensor will be different for a single particle compared to two collinear particles, if the total momentum is the same in each case. Note that it is possible to obtain an infrared safe version of sphericity called *linearised sphericity*, given by [48]:

$$S^{\alpha\beta} = \frac{\sum_i \frac{p_i^{\alpha} p_i^{\beta}}{|\mathbf{p}_i|}}{\sum_i |\mathbf{p}_i|} \quad (83)$$

Even though there is this important difference between thrust and sphericity, we will calculate both in our results since both options have been used in the past to measure the average p_{\perp} .

First of all, the average p_{\perp} will be plotted again as a function of $\Delta\kappa_{max}$, this time with respect to the sphericity axis:

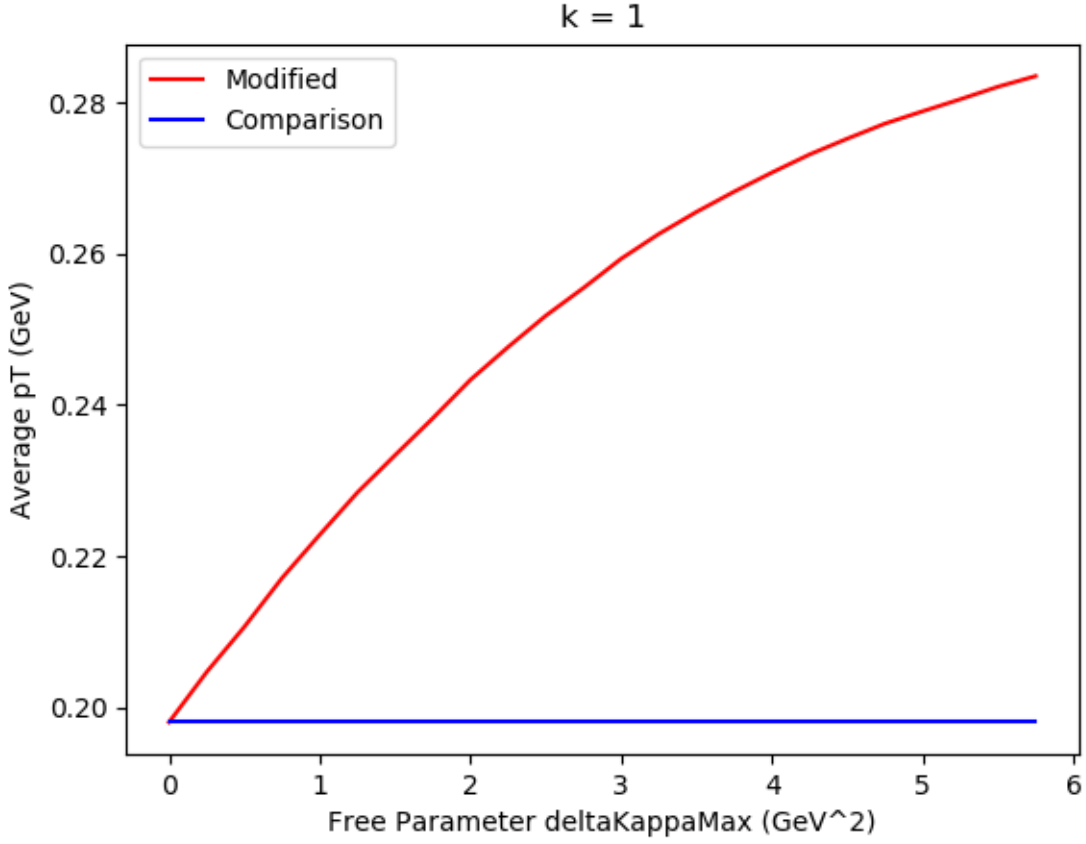


Figure 24: Change in average p_{\perp} with respect to sphericity axis as a function of $\Delta\kappa_{max}$ at $k = 1$.

There remains a clear increase in average p_{\perp} as the string tension is increased, though the increase is around 50% rather than nearly double as was the case when measuring along the string axis. We expect any effects of our model to be reduced in this way when measuring with respect to an experimental axis. The experimental axis cannot exactly replicate the actual string axis, and so the full increase in average p_{\perp} will not be completely carried through. A plot of average p_{\perp} with respect to the thrust axis results in a similar increase in average p_{\perp} .

There is one last step to be taken to have an entirely realistic simulation of electron-positron collisions, and that is to turn on hadron decays and final state radiation. The plot of average p_{\perp} as a function of $\Delta\kappa_{max}$ then becomes:

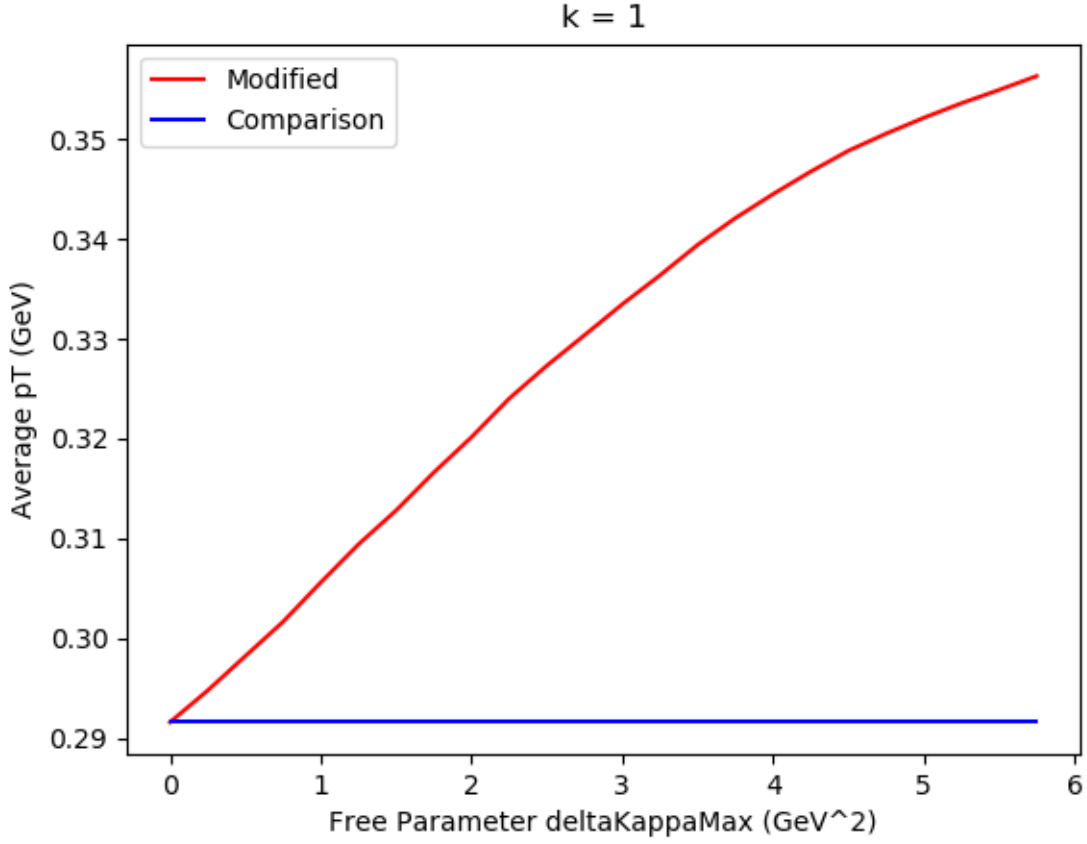


Figure 25: Change in average p_{\perp} with respect to sphericity axis as a function of $\Delta\kappa_{max}$ with hadron decay and final state radiation on.

With hadron decays and final state radiation in place, the increase in average p_{\perp} is further reduced. However, the increase is not completely washed out, since it now reaches around a 15% increase compared to the zero temperature value at high $\Delta\kappa_{max}$.

We can now see what the relationship between p_{\perp} and strangeness looks like when measuring the p_{\perp} with respect to an experimental axis. For the sake of using both thrust and sphericity, the next plot will be performed by measuring with respect to the thrust axis, though similar results were obtained for sphericity. Plotting the average p_{\perp} ratio to pions as a function of function of $\Delta\kappa_{max}$ for the same types of hadrons as before:

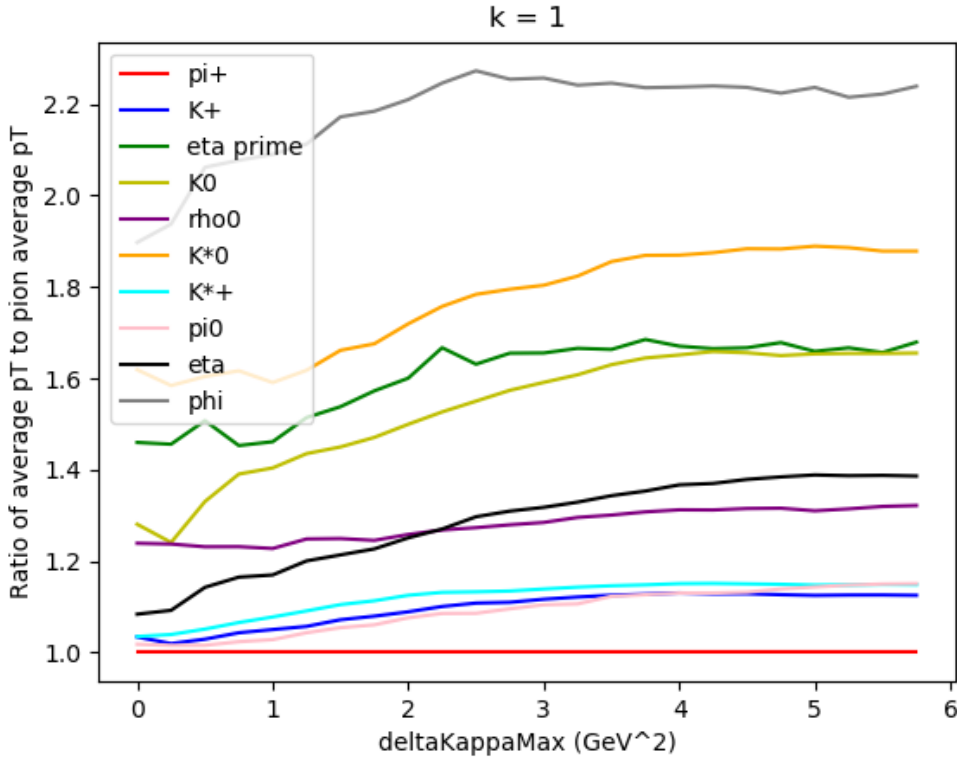


Figure 26: Average p_{\perp} ratio to pions as a function of $\Delta\kappa_{max}$ for different mesons with respect to thrust axis.

Measuring with respect to the thrust axis seems to amplify the difference between charged and uncharged particles, since the charged kaons begin much lower than the neutral kaons and grow at a slower comparative rate. The neutral pion also seems to have an increasing p_{\perp} compared to the charged pion, highlighting a difference that wasn't present when measuring exactly along the string axis. This difference between charged and uncharged particles is most likely to be a result of the mechanics involved in thrust and sphericity, and is therefore irrelevant to our study of the effects of our enhanced string tension. The more interesting result is that the ϕ meson, along with the charged kaons and η mesons, have an average p_{\perp} that increases at a faster rate than the hadrons without strange content, ignoring charged particles. The π^0 and ρ mesons are clearly increasing by less than the neutral strange mesons, implying that there is still a measureable difference in average p_{\perp} between strange and non-strange mesons.

7 Conclusion

We have developed in this thesis a model for hadronisation that incorporates a time dependent thermal string tension, based on the highly successful Lund model. This modification has been implemented using an easily accessible plug-and-play `UserHook` code. In doing so, we

have demonstrated that more strange quarks will be produced with enhanced transverse momentum at early times, when the string is “hottest.” This will result in an increased average p_{\perp} for strange hadrons compared to non-strange hadrons, as seen within the PYTHIA particle collision simulator. Such an effect should therefore be measurable in electron-positron collisions. The primary difficulty in observing this effect is isolating the different types of hadrons, so that the average p_{\perp} can be compared between different species. However, the presence of a clear enhancement of average p_{\perp} in neutral kaons and ϕ mesons would be significant motivation to attempt an analysis of existing electron-positron data to see if such a difference exists.

This project could be extended to consider a possible dependence of the string tension on an environment variable. We have already seen that an enhanced string tension leads to increased strangeness. If the string tension could be further enhanced by the presence of nearby strings, for example, then we would predict an increase in strangeness when more particles are present in an event. This could go some way to explaining the dependence of strangeness on particle multiplicity in proton-proton collisions seen in figure 2. Before attempting this, a description of diquarks would need to be included in our model, since we have not studied the generation of baryons in this thesis.

Appendices

A Derivation of H and f Distributions

In order to determine H and f , we will set eq.(28) and eq.(29) equal to one another. Taking the natural logarithm of both sides, and letting $h(\Gamma) = \ln(H(\Gamma))$, $g(z) = \ln(zf(z))$:

$$h(\Gamma_1) + g(z_+) = h(\Gamma_2) + g(z_-) \quad (84)$$

Taking partial derivatives of both sides with respect to z_+ and then z_- will remove all the dependence on g . We are eventually left with:

$$\frac{dh(\Gamma_1)}{d\Gamma_1} + \Gamma_1 \frac{d^2h(\Gamma_1)}{d\Gamma_1^2} = \frac{dh(\Gamma_2)}{d\Gamma_2} + \Gamma_2 \frac{d^2h(\Gamma_2)}{d\Gamma_2^2}. \quad (85)$$

In order to find this equation, the chain rule was used, along with eq.(26):

$$\frac{\partial h(\Gamma_1)}{\partial z_+} = \frac{dh(\Gamma_1)}{d\Gamma_1} \frac{\partial \Gamma_1}{\partial z_+} = \frac{dh(\Gamma_1)}{d\Gamma_1} \left(-\frac{m^2(1-z_-)}{z_-z_+^2} \right). \quad (86)$$

Reversing the product rule:

$$\frac{\partial}{\partial \Gamma_1} \left(\Gamma_1 \frac{\partial h_1}{\partial \Gamma_1} \right) = \frac{\partial}{\partial \Gamma_2} \left(\Gamma_2 \frac{\partial h_2}{\partial \Gamma_2} \right), \quad (87)$$

Since the left side only depends on Γ_1 and the right side only depends on Γ_2 , this equation can only be satisfied if each side individually is equal to a constant. Let this constant be called $-b$, and drop indices 1 and 2 since the equation holds for both sides:

$$\frac{\partial}{\partial \Gamma} \left(\Gamma \frac{\partial h}{\partial \Gamma} \right) = -b \quad (88)$$

Integrating both sides and rearranging:

$$h(\Gamma) = -b\Gamma + a \ln(\Gamma) + \ln(C), \quad (89)$$

a and C are arbitrary constants of integration. Exponentiating both sides:

$$H(\Gamma) = C\Gamma^a \exp(-b\Gamma). \quad (90)$$

This is the form of the distribution H we wanted to obtain. Since H is a probability distribution, the constant C acts as a normalisation constant.

We can now find the distribution f by substituting eq.(97) into eq.(92). After rearranging so that left side depends only on z_+ and right side depends only on z_- :

$$\begin{aligned}
g(z_+) + \frac{bm^2}{z_+} - a_1 \ln\left(\frac{m^2}{z_+}\right) - a_2 \ln\left(\frac{1-z_+}{z_+}\right) + \ln(C_1) \\
= g(z_-) + \frac{bm^2}{z_-} - a_2 \ln\left(\frac{m^2}{z_-}\right) - a_1 \ln\left(\frac{1-z_-}{z_-}\right) + \ln(C_2),
\end{aligned}$$

Since each side only depends on z_+ or z_- , the same reasoning as for distribution H can be used to equate both sides to a constant. Let this constant be n , and then exponentiate both sides dropping indices [26]:

$$f(z) = N \frac{1}{z} (1-z)^a \exp\left(\frac{-bm^2}{z}\right) \quad (91)$$

Here, $N = \exp(n)$, representing a normalisation constant. The same parameters a and b from $H(\Gamma)$ appear in this distribution.

B Lorentz Invariance of Proper Time

It can be readily proven that the quantity $\tau = \sqrt{t^2 - x^2}$ is Lorentz invariant, as is required for τ to define a proper time. Under a Lorentz boost by velocity v in the x direction, the temporal component transforms as $t' = \gamma(t - vx)$, and the spatial coordinate transforms as $x' = \gamma(x - vt)$, where $\gamma = \frac{1}{\sqrt{1-v^2}}$. τ therefore transforms as:

$$\tau' = \sqrt{\gamma^2((t - vx)^2 - (x - vt)^2)} \quad (92)$$

$$\tau' = \gamma \sqrt{t^2 - 2vxt + v^2x^2 - x^2 + 2xvt - v^2x^2} \quad (93)$$

$$\tau' = \gamma \sqrt{(1 - v^2)(t^2 - x^2)} \quad (94)$$

Since $\gamma = \frac{1}{\sqrt{1-v^2}}$:

$$\tau' = \sqrt{t^2 - x^2} = \tau \quad (95)$$

τ is therefore unchanged under a Lorentz boost, meaning it is appropriate to describe τ as a proper time.

C Gaussian Sampling Problem

Setting eq.(79) and eq.(80) equal to one another:

$$\frac{2p_{\perp}\pi}{\kappa_0} \exp\left(\frac{-\pi p_{\perp}^2}{\kappa_0}\right) = \frac{2p_{\perp}\pi}{\kappa_{therm}} \exp\left(\frac{-\pi p_{\perp}^2}{\kappa_{therm}}\right) \quad (96)$$

$$\exp\left(-\pi p_{\perp}^2\left(\frac{1}{\kappa_0} - \frac{1}{\kappa_{therm}}\right)\right) = \frac{\kappa_0}{\kappa_{therm}} \quad (97)$$

$$\pi p_{\perp}^2\left(\frac{1}{\kappa_{therm}} - \frac{1}{\kappa_0}\right) = \ln\left(\frac{\kappa_0}{\kappa_{therm}}\right) \quad (98)$$

$$\pi p_{\perp}^2\left(\frac{1}{\kappa_0} - \frac{1}{\kappa_{therm}}\right) = \ln\left(\frac{\kappa_{therm}}{\kappa_0}\right) \quad (99)$$

Multiplying left hand side by $\frac{\kappa_{therm}}{\kappa_{therm}}$:

$$\frac{\pi p_{\perp}^2}{\kappa_{therm}}\left(\frac{\kappa_{therm}}{\kappa_0} - 1\right) = \ln\left(\frac{\kappa_{therm}}{\kappa_0}\right) \quad (100)$$

Solving for p_{\perp} :

$$p_{\perp} = \sqrt{\frac{\kappa_{therm} \ln\left(\frac{\kappa_{therm}}{\kappa_0}\right)}{\pi\left(\frac{\kappa_{therm}}{\kappa_0} - 1\right)}} \quad (101)$$

Since $\frac{\kappa_{therm}}{\pi}$ is equal to the enhanced width σ_{therm}^2 :

$$p_{\perp} = \sigma_{therm} \sqrt{\frac{\ln\left(\frac{\kappa_{therm}}{\kappa_0}\right)}{\left(\frac{\kappa_{therm}}{\kappa_0} - 1\right)}} \quad (102)$$

For a thermal string tension that is double the normal string tension, we find $p_{\perp} = 0.833\sigma_{therm}$. This means that if we set the probability to be 1 above the intersection point, then we are actually only sampling 83.3% of the enhanced Gaussian, and the rest we are just accepting blindly. Ideally, we would like to sample at least 95% of the distribution since that corresponds to 2 standard deviations either side of the mean. This information loss becomes worse if we increase the ratio of tensions (triple the tension is 74.1%, quadruple is 68.0%, and so on).

D UserHook Code

```
#include "Pythia8/Pythia.h"
using namespace Pythia8;

//New free parameter definitions
double deltaKappaMax = -0.25; //Kappa' maximum minus ordinary kappa
double k = 1; //Former tau0 divided by average unmodified tau

//Average tau calculated by brute force
double tauAverage = 1.2152;

//Declare StringPT object used to reset pT after modifications
```

```

StringPT pTSaved;

//Declare Settings object to be modified
Settings settingsMod;

//Declare original string tension globally
double kappaOld = 0;

//Declare UserHooks class
class MyUserHooks : public UserHooks {
public:

    //Constructor and Destructor
    MyUserHooks() {}
    ~MyUserHooks() {}

    //Enable Modified Hadronization UserHook methods
    virtual bool canChangeFragPar() {return true;}

    //Change pT Spectrum Width
    virtual bool doChangeFragPar(StringFlav* flavPtr, StringZ* zPtr,
        StringPT* pTPtr, int idEnd, double m2Had, vector<int> iParton,
        const StringEnd* sEnd) override {

        pTSaved = *pTPtr; //Save original pT given by Pythia
        settingsMod = *settingsPtr; //Define settings to be modified
        sigmaOld = settingsPtr->parm("StringPT:sigma"); //Keep track of original sigma
        kappaOld = pow2(sigmaOld)*M_PI; //Calculate original string tension

        //Gamma of vertex
        double gamma = sEnd->GammaNew;

        //Tau of vertex
        double tau = 0.5*((-deltaKappaMax*k*tauAverage/kappaOld)+(sqrt(gamma)/kappaOld)
            -k*tauAverage+sqrt((pow2(deltaKappaMax*k*tauAverage)/pow2(kappaOld))-
            2*(deltaKappaMax*k*tauAverage*sqrt(gamma)/pow2(kappaOld))+(gamma/pow2(kappaOld))
            +(2*deltaKappaMax*k*tauAverage*k*tauAverage/kappaOld)
            +(2*sqrt(gamma)*k*tauAverage/kappaOld)+pow2(k*tauAverage)));

        //New tau-dependent kappa
        double kappaNew = kappaOld + deltaKappaMax*k*tauAverage/(tau+k*tauAverage);

        //New modified pT width
        double sigmaNew = sqrt(kappaNew/M_PI);

        //Modify pT width in settings object
        settingsMod.parm("StringPT:sigma",sigmaNew);

        //Reinitialise
        pTPtr->init(settingsMod, particleDataPtr, rndmPtr, infoPtr);
        return true;
    }
}

//Veto Algorithm for strangeness ratio

```

```

virtual bool doVetoFragmentation(Particle had, const StringEnd* sEnd) {

    //Ratio of getting strange quark
    double probStoUD = settingsPtr->parm("StringFlav:probStoUD");

    //Gamma of vertex
    double gamma = sEnd->GammaNew;

    //Tau of vertex
    double tau = 0.5*((-deltaKappaMax*k*tauAverage/kappaOld)+(sqrt(gamma)/kappaOld)
-k*tauAverage+sqrt((pow2(deltaKappaMax*k*tauAverage)/pow2(kappaOld))-
2*(deltaKappaMax*k*tauAverage*sqrt(gamma)/pow2(kappaOld))+(gamma/pow2(kappaOld))
+(2*deltaKappaMax*k*tauAverage*k*tauAverage/kappaOld)
+(2*sqrt(gamma)*k*tauAverage/kappaOld)+pow2(k*tauAverage)));

    //New tau-dependent kappa
    double kappaNew = kappaOld + deltaKappaMax*k*tauAverage/(tau+k*tauAverage);

    //Veto algorithm (return true is a veto)
    if ((abs(sEnd->flavNew.id) == 2) &&
(rndmPtr->flat() < 1-(probStoUD)/(pow(probStoUD, kappaOld/kappaNew)))) return true;
    if ((abs(sEnd->flavNew.id) == 1) &&
(rndmPtr->flat() < 1-(probStoUD)/(pow(probStoUD, kappaOld/kappaNew)))) return true;

    //Restore content of StringPT to its original value for the rest of Pythia
    StringPT* pTPtr = sEnd->pTSELPtr;
    *pTPtr = pTSSaved;

    return false;
}

private:
};

```

References

- [1] Skands, P, 2017. *Introduction to QCD*, arXiv:1207.2389.
- [2] Ellis, J 2014. 'The Discovery of the Gluon', *World Scientific Review*, arXiv:1409.4232.
- [3] Dissertori, G, Knowles, I and Schmelling, M 2009. *Quantum Chromodynamics: High Energy Experiments and Theory*, 'Chapter 3: Theory of QCD', Oxford University Press, Oxford.
- [4] Wilson, K 1975. 'The renormalization group: Critical phenomena and the Kondo problem', *Reviews of Modern Physics*, Vol. 47, No. 4, pp. 773-840.
- [5] ETM Collaboration 2012. 'Strong Running Coupling at τ and Z_0 Mass Scales from Lattice QCD', *Physical Review Letters*, Vol. 108, 262002.
- [6] Sommerfeld, A 1923. *Atomic Structure, Spectral Lines*, Methuen Press, London.
- [7] Jaffe, A and Witten, E, 2000. *Quantum Yang-Mills Theory*.
- [8] Andersson, B, Gustafson, G, Ingelman, G and Sjöstrand, T 1983. 'Parton Fragmentation and String Dynamics', *Physics Reports*, Vol. 97, No. 2, pp. 31-145.
- [9] Meyer, H 2015. 'Lattice QCD: A Brief Introduction', *Lattice QCD for Nuclear Physics*, Lecture Notes in Physics 889.
- [10] Bali, G and Schilling, K 1992. 'Static quark-antiquark potential: Scaling behaviour and finite-size effects in SU(3) lattice gauge theory', *Physical Review D*, Vol. 46, No. 6, pp. 2637-2646.
- [11] Fredenhagen, K and Marcu, M 1986. 'Confinement Criterion for QCD with Dynamical Quarks', *Physical Review Letters*, Vol. 56, No. 3, pp. 223-224.
- [12] Ferreres-Solé, S, Sjöstrand, T 2018. 'The space-time structure of hadronization in the Lund model', *The European Physical Journal C*, Vol. 78:983.
- [13] Artru, X and Mennessier, G 1973. 'String Model and Multiproduction', *Nuclear Physics*, Vol. B70, pp. 93-115.
- [14] Seymour, M and Marx, M 2013. *Monte Carlo Event Generators*, arXiv:1304.6677.
- [15] Sjöstrand, T, Mrenna, S and Skands, P 2008. 'A brief introduction to PYTHIA 8.1', *Computer Physics Communications*, Vol. 178(11), pp. 852-867.
- [16] TASSO Collaboration, 1979. 'Evidence for Planar Events in e^+e^- Annihilation at High Energies', *Physics Letters B*, Vol.86, No.2, pp.243-249.
- [17] ALICE Collaboration, 2017. 'Enhanced production of multi-strange hadrons in high-multiplicity proton-proton collisions', *Nature Physics*, Vol. 13, No.1, pp. 535-539.

- [18] Gebert, M 2016. *Something Strange? A glance into Parton Fragmentation*, PHS3350 Undergraduate Research Project, Physics Dept. Monash University.
- [19] Andersson, B 1998. 'The Lund Model', in Ericson T and Landshoff P (ed.), *Cambridge Monographs on Particle Physics, Nuclear Physics and Cosmology*, Cambridge University Press, Cambridge.
- [20] Ferreres-Sole, S and Sjöstrand, T 2018. 'The space-time structure of hadronization in the Lund model', *The European Physical Journal C*, Vol.78, No.1, Chapter 983.
- [21] Gurvich, E 1979. 'The quark-antiquark pair production mechanism in a quark jet', *Physics Letters B*, Vol. 87, No. 4, pp. 386-388.
- [22] Penin, A 2010. 'Measuring Vacuum Polarization with Josephson Junctions', *Physical Review Letters*, Vol. 104, Chapter 9.
- [23] Schwinger, J 1951. 'On Gauge Invariance and Vacuum Polarization', *Physical Review*, Vol. 82, No. 5, pp. 664-679.
- [24] Sjöstrand, T, Mrenna, S and Skands, P 2006. 'PYTHIA 6.4 Physics and Manual', *Journal of High Energy Physics*, Vol 2006(5), 026.
- [25] Linsefors, L and Barrau, A 2015. 'Restrictions on curved cosmologies in modified gravity from metric considerations', *Physics Letters B*, Vol. 748, No.1, pp. 295-300.
- [26] Sjöstrand, T 1984. 'The merging of jets', *Physics Letters*, Vol. 142B, No. 5-6, pp. 420-424.
- [27] Becattini, F 1995. 'A thermodynamical approach to hadron production in e^+e^- collisions', *Zeitschrift für Physik C Particles and Fields*, Vol. 69, No. 3, pp. 485-492.
- [28] ATLAS Collaboration, 2016. 'Observation of long-range elliptic azimuthal anisotropies in $\sqrt{s} = 13$ and 2.76 TeV pp collisions with the ATLAS detector', *Physical Review Letters*, Vol. 116, 172301.
- [29] Braun-Munzinger, P and Stachel, J 2007. 'The quest for the quark-gluon plasma', *Nature*, Vol. 448, pp. 302-309.
- [30] Berges, J, Floerchinger, S and Venugopalan, R 2018. 'Dynamics of entanglement in expanding quantum fields', *Journal of High Energy Physics*, Vol. 2018(4), 145.
- [31] Calabrese, P and Cardy, J 2004. 'Entanglement Entropy and Quantum Field Theory', *Journal of Statistical Mechanics: Theory and Experiment*, P06002.
- [32] Bonderson, P, Knapp, C and Patel, K 2017. 'Anyonic Entanglement and Topological Entanglement Entropy', *Annals of Physics*, Vol. 385, pp. 399-468.
- [33] Lesne, A and Laguës, M 2012. *Scale Invariance: From Phase Transitions to Turbulence*, Chapter 7, Springer, Berlin Heidelberg.

- [34] Antonov, D, Del Debbio, L and Di Giacomo, A 2003. 'A model for string-breaking in QCD', *Journal of High Energy Physics*, JHEP08(2003).
- [35] Brandt, E, Mikitik, G and Zeldov, E 2009. 'Nanomechanics of an individual vortex in an anisotropic type-II superconductor', *Physical Review B*, Vol. 80, 054513.
- [36] Assi, H, Chaturvedi, H, Dobramysl, U, Pleimling, M and Täuber, U 2015. 'Relaxation Dynamics of Vortex Lines in Disordered Type II Superconductors Following Magnetic Field and Temperature Quenches', *Physical Review E*, Vol. 92, 052124.
- [37] Pirner, H, Kopeliovich, B and Reygers, K 2018. *Strangeness Enhancement due to String Fluctuations*, arXiv: 1810.04736.
- [38] Gavrilov, V, Kodolova, N and Lychkovskaya, N 2010. 'Jet transverse structure as a test of hadronization models', *Journal of Physics G: Nuclear and Particle Physics*, Vol. 37, 075009.
- [39] CLAS Collaboration 2014. 'Strangeness Suppression of $q\bar{q}$ Creation Observed in Exclusive Reactions', *Physical Review Letters*, Vol. 113, 152004.
- [40] Lonnblad, L 2012. *Fooling around with the Sudakov Veto Algorithm*, arXiv: 1211.7204.
- [41] Mrenna, S and Skands, P 2016. 'Automated Parton-Shower Variations in Pythia 8', *Physical Review D*, Vol. 94(7).
- [42] STAR Collaboration 2006, 'Strange Particle Production in $p + p$ Collisions at $\sqrt{s} = 200$ GeV', *Physical Review C* Vol. 75, 064901.
- [43] Karneyeu, A, Mijovic, L, Prestel, S and Skands, P 2014. 'MCPLOTS: a particle physics resource based on volunteer computing', *The European Physical Journal C*, Vol. 74(2), pp. 2714(22).
- [44] Skands, P, Carrazza, S and Rojo, J 2014. 'Tuning PYTHIA 8.1: The Monash 2013 Tune', *The European Physical Journal C* Vol.74(8).
- [45] Bjorken, J and Brodsky, S 1970. 'Statistical Model for Electron-Positron Annihilation into Hadrons', *Physical Review D*, Vol. 1, pp.1416-1420.
- [46] Brandt, S, Peyrou, C, Sosnowski, R and Wroblewski, A 1964. 'The principal axis of jets-an attempt to analyse high-energy collisions as two-body processes', *Physics Letters*, Vol. 12, pp.57-61.
- [47] Salam, G 2010. 'Towards Jetography', *The European Physical Journal C*, Vol. 67(3), pp.637-686.
- [48] Parisi, G 1978. 'Superinclusive cross sections', *Physics Letters B*, Vol. 74, pp.65-67.